Spring 2019

Path Loss Models for Two Small Airport Indoor Environments at 31 GHz

Alexander L. Grant

Path Loss Models for Two Small Airport Indoor Environments at 31 GHz

by

Alexander L. Grant

Bachelor of Science
The Citadel, 2017

Submitted in Partial Fulfillment of the Requirements

For the Degree of Master of Science in

Electrical Engineering

College of Engineering and Computing

University of South Carolina

2019

Accepted by:

David W. Matolak, Director of Thesis

Mohammod Ali, Reader

Cheryl L. Addy, Vice Provost and Dean of the Graduate School

DEDICATION

To my parents, younger brother and all those who have helped me along the way.

ACKNOWLEDGEMENTS

It has been a wonderful journey here while perusing my Master's degree. This effort has been a challenge, requiring constant motivation and proactivity. However, there were many individuals on my side supporting me.

First, I would like to thank Dr. Matolak for his guidance and willingness to give me the opportunity to do research here. He continuously gave good advice and prepared me well through his teachings. Dr. Matolak also kept me on schedule throughout the two years of my study so that I could succeed in a timely manner. I am forever grateful for his patience and the opportunity to be a student of a great engineer.

Thank you to all members of the committee who have also served as my mentors when I needed them.

Finally, I would like to thank my parents and my younger brother for their continuous moral support. I would not have made it this far without any of you.

ABSTRACT

Path loss modeling plays a fundamental role in the design of fixed and mobile communication systems for a range of applications. Another term for path loss is channel attenuation, or reduction in signal power from transmitter to receiver. Work here was in support of a NASA project for advanced air traffic management (ATM) applications, specifically for improving the efficiency of airports. Measurements in the millimeter wave (mmWave) band were conducted at 31 GHz in indoor settings at a small municipal airport, the Jim Hamilton–L.B. Owens Airport, in Columbia, SC. Some measurements were also taken at 5 GHz for comparison. A combination of line of sight (LOS) and non-line of sight (NLOS) measurements were taken throughout two airport buildings. This includes inside the terminal building on both floors and inside a maintenance hangar. After samples were taken, path loss models were computed. As expected, 5 GHz signals show less attenuation than the 31 GHz signals, and both signals are influenced by nearby indoor objects. For both the terminal building and the maintenance hangar, path loss exponents were larger than the free space value of two, and standard deviations of the model fits slightly larger than those found for indoor office environments.

TABLE OF CONTENTS

DEDICATION..... iii

ACKNOWLEDGEMENTS..... iv

ABSTRACT.....v

LIST OF TABLES.....vii

LIST OF FIGURES.....ix

CHAPTER 1: INTRODUCTION.....1

CHAPTER 2: BASIC PHYSICS, PRINCIPLES AND PROPAGATION MODELS……9

CHAPTER 3: PRE-TEST MEASUREMENTS……...…..……24

CHAPTER 4: AIRPORT EXPERIMENT SETUP FOR 5 AND 31 GHZ……...…….34

CHAPTER 5: AIRPORT MEASUREMENT RESULTS AND ANALYSIS.....39

CHAPTER 6: CONCLUSION……..……...….53

References……..54

Appendix A: Photographs of Equipment used in all Experiments……....56

Appendix B: Tables for pre-test, Airport, Main Building and Hangar Measurements…..61

LIST OF TABLES

Table 4.1 Equipment required for airport channel measurements……35

Table 5.1 CI path loss model parameters, standard deviation and path loss exponents of all Indoor runs (NLOS main building)……..46

Table 5.2 Results showing standard deviation and pathloss exponents of previous outdoor and hangar runs……..52

Table B.1 Received Power in dBm vs. distance in meters (Sweringen Parking Lot at 31 GHz for co-polarized setting) ……...61

Table B.2 Received Power in dBm vs. distance in meters (Sweringen Parking Lot at 31 GHz for cross-polarized setting….....62

Table B.3 Received Power(dBm), Average Power(dBm), real loss (dB) and Free space path loss(dBm) vs distance in meters in Hallway at 5 GHz…….…….……63

Table B.4 Received Power (dBm) and Average Power(dBm) vs. distance in meters for Hallway at 31 GHz…….……...63

Table B.5 Loss in dB vs distance in meters in Airport main building at 31 GHz for Run #1……..…..……64

Table B.6 Loss in dB vs distance in meters in Airport main building at 31 GHz for Run #2……..…….……64

Table B.7 Loss in dB vs distance in meters in Airport main building at 31 GHz for Run #3…….……..65

Table B.8 Power in dBm vs distance in meters in Airport main building at 31 GHz for Run #4…….…….…65

Table B.9 Measured Power in dBm vs. distance in meters in Airport main building at 31 GHz for Run #5……..…….……..66

Table B.10 Measured Power in (dBm) vs. distance in meters at Hangar for 31 GHz LOS Run #1……..……66

Table B.11 Measured Power in (dBm) vs. distance in meters at Hangar for 31 GHz NLOS Run #1 ……...…….……..67

Table B.12 Measured Power in (dBm) vs distance in meters at Hangar for 31 GHz Run #2……..…….67

Table B.13 Measured Power in (dBm) vs distance in meters Hangar for 31 GHz Run #3……...……...68

Table B.14 Measured Power in (dBm) vs distance in meters Hangar for 31 GHz Run #4……...……...…..68

Table B.15 Measured Power in (dBm) vs distance in meters Hangar for 31 GHz Run #5……..…….……...……..68

Table B.16 Measured Power in (dBm) vs distance in meters Hangar for 31 GHz Run #6……69

LIST OF FIGURES

Figure 3.1 Rohde and Schwartz equipment on desk……..…….……..25

Figure 3.2 Outdoor receiver setup in Swearingen Parking Lot……..…….…..…28

Figure 3.3 Path loss in dB vs. logarithm of distance in meters, for the co polarized measurements in the Swearingen parking lot, for frequency 31 GHz. Free-space and simplified two-ray path losses also shown ……...…….29

Figure 3.4 Path loss in dB vs. logarithm of distance in meters, for the cross polarized measurements in the Swearingen parking lot, for frequency 31 GHz. Free-space and simplified two-ray path losses also shown.....……..30

Figure 3.5 Path loss in dB versus logarithm of distance in m for 5 GHz, in 3rd floor D-wing hallway. Free Space path loss (FSPL) also shown……...32

Figure 3.6 Measured 31 GHz Plot of Path Loss and Free Space vs logarithm of distance for 31 GHz in 3rd floor D-wing hallway……33

Figure 4.1 Diagram of test configuration showing transmit to receive signal flow……..36

Figure 5.1 LOS Measured Power, Average Power and FSPL vs logarithm of distance in the Main building at 31 GHz for Run #1 …….…….39

Figure 5.2 LOS Measured Power, Average Power and FSPL vs logarithm of distance in the Main building at 31 GHz for Run #2 ……..……..……..40

Figure 5.3 LOS Measured Power, Average Power and FSPL vs logarithm of distance in the Main building at 31 GHz for Run #3……..……..…….……..41

Figure 5.4 Combined Average of Power Measurements from previous 3 runs at 31 GHz……...42

Figure 5.5 NLOS CI model of Power measurements in dBm taken in two rooms in the main building at 31 GHz.……...……..…….…….43

Figure 5.6 NLOS CI model of Power measurements in dBm taken in a room and from below the transmitter on a lower floor in the main building at 31 GHz……...……44

Figure 5.7 NLOS CI model of previous two sets of Power measurements in dBm taken in the main building at 31 GHz……...……...……..……..45

Figure 5.8 CI model of LOS/NLOS Power measurements in dBm and Free Space vs the logarithm of distance in Hangar at 31 GHz Run 1……..…….…….……47

Figure 5.9 CI model of LOS/NLOS Power measurements in dBm and Free Space vs the logarithm of distance in Hangar at 31 GHz Run 2…..……..….48

Figure 5.10 CI model of LOS/NLOS Power measurements in dBm and Free Space vs the logarithm of distance in Hangar at 31 GHz Run 3……..……..…….49

Figure 5.11 CI model of NLOS Power measurements in dBm and Free Space vs the logarithm of distance Outdoors near hangar at 31 GHz Run 4…….……50

Figure 5.12 Combined CI model of four previous LOS/NLOS Power measurements in dBm and Free Space vs the logarithm of distance at 31 GHz…….…..51

Figure A.1 Photograph of signal and spectrum analyzer (left) and vector signal generator (right)…….52

Figure A.2 31 GHz Horn Antenna…….53

Figure A.3 Microwave Dynamics Amplifier.……53

Figure A.4 5 GHz Omni-directional Antenna……54

Figure A.5 Microwave Dynamics Mixer……..…….54

Figure A.6 Antenna mount set up for Transmitter…….55

Figure A.7 Cart with Receiver Equipment and Power Supplies……55

Figure A.8 1500 W Power Inverter……56

Figure A.9 Marine 12 V DC Battery…….56

CHAPTER 1

INTRODUCTION

1.1 Motivation and Background

Wireless applications and technologies play an integral part in modern day society. Since the invention of the wireless telegraph by Marconi [1], governments, corporations, the public, and militaries around the world have been developing new ways to take advantage of this technology. During World War II, experimentation in and use of wireless devices had a significant influence on the course of global history. Remote controlled vehicles were used by the U.S Army and Navy as early as the 1940's [1]. In cases where personnel were unable to control a ship, a nearby ship had the capability to control this vessel with electromagnetic signals. In addition, remotely controlled aircraft were used as test targets during training or experiments. Communication schemes used today such as direct sequence spread spectrum (DSSS) and frequency hopping were also first developed and used during World War II [1]. During the Cold War, channel sounders used direct sequence spread spectrum to detect distant phenomena such as nuclear explosions, earthquakes and rocket launches via Doppler shifted signals [1]. The magnitude of new developments over time is vast and continues to grow with new problems and new demands.

Today, billions of people worldwide use wireless devices from smartphones and Wi-Fi, to vehicular radios and satellite television. One of the fastest growing applications

in wireless technologies is the internet of things (IoT). Current uses of devices connected to the IoT include cloud computing, mobile communication, and video streaming. As modern nations find more uses for wireless technologies and developing countries add new users to the current network infrastructure, much hardware will have to be upgraded to support more devices. By the year 2045, it is predicted that wireless networks around the U.S will reach a significant portion of the Shannon capacity limit [2]. Therefore, the capacity of networks and their devices must be increased.

For this reason, wireless companies are investigating shifting to (and/or adding) higher frequency bands that are currently either unused or used in inefficient ways. There are several different higher frequency bands that are being investigated. These include bands in the millimeter wave (e.g., 30, 60, and 90 GHz) and optical frequency ranges. The most common way to carry optical signals is with optical fiber. However, having a device connected to a fiber does not easily allow its communication to be mobile, thus optical wireless, or "free-space optical" (FSO) systems are also being researched. Research in millimeter wave technologies is being conducted for use in applications that require movement of a device and which may not permit the extremely narrow beams of FSO systems.

There are several advantages to using millimeter wave signals. Millimeter wave signals tend to travel in relatively narrow beams when using directional antennas, rather than spreading in all directions as is common for omnidirectional antennas used at lower frequencies. The use of narrow beams makes it more difficult for a malicious entity to eavesdrop on communications or jam signals. In addition, interception of communications between two millimeter wave antennas can potentially easily be monitored. If one were to

attempt eavesdropping or jamming of a millimeter wave system, it might be easier to detect since the intercepting device would need to be positioned near to the line of sight (LOS) of both antennas. Also, because the wavelengths of signals used by these systems are on the order of millimeters, antennas can be made relatively small. This allows multiple antennas to fit on one chip or compact device. Another characteristic of millimeter wave systems that researchers are interested in is their suitability for direction finding and tracking. This is because multiple small antennas in a compact device can not only steer the direction of transmitted signals without moving the transmitter itself, but such antennas can more easily find the direction of incoming beams than non-directional antennas. For this reason, researchers at many universities and telecommunications companies are investigating the use of millimeter wave antennas in mobile cellular and other wireless networks. The goal of this research is to develop methods for increasing the efficiency and capacity of these networks.

To improve bandwidth efficiency of the network, multiple users associated with one cell tower or base station can occupy their own time slots, and/or frequency channel and/or spatial beam. As the user device moves, a cell tower will track its location over time and steer one of its antenna beams toward the user. The cell tower can also steer multiple beams to several users at once while they are moving, ideally without crossing the beams. In case beams do need to cross, beams may need to switch among different frequency bands rapidly. This allows communication to take place with minimal interference between users. Since these cellular systems are moved to higher frequency bands, the total available bandwidth increases. This in turn increases its capacity.

In other future applications, airports may also need to make use of millimeter wave systems. As developing nations continue to add new aircraft to the airspace, the density of aircraft within the airspace will increase. Therefore, today's communication systems for air-ground and airport surface systems may not have the capability to maintain the same quality of service and security in the future. In light of this, NASA is funding research efforts to design and test new systems that will extend the capacity of the current air traffic management infrastructure.

Recently, several deployments and experiments using mmWave technologies were reported for airport surface applications. One development is a 60 GHz unlicensed indoor system at the Tokyo-Narita airport. It was combined with Mobile Edge Computing (MEC) to enable ultra-high speed content download with low latency. It is planned to be deployed in 2020 during the winter Olympic games [3]. In the same NASA project that supported the work in this thesis, an experiment done by Boise State University measured 60 GHz channel characteristics at the Boise, Idaho airport. From their measurements, Boise State also produced pathloss models for that environment in line of sight (LOS) and non-line of sight (NLOS) settings [4].

1.2 Literature Review

Past wireless measurements and experiments in the millimeter wave band will be discussed in this section. Multiple analyses, simulations, and measurements have been done to get a better understanding of the propagation characteristics of mmWave signals [2], [4], [5]. However, more data will be needed before full implementation of a new

wireless network can take place at local airports. This is because much previous work relied on analytic models or ray tracing software that assumed that propagation is dominated by LOS with low powered reflections [2]. Multiple mmWave frequency bands must be considered, and a larger variety of airport settings must be investigated.

With their larger bandwidths, millimeter wave systems can increase the capacity of future networks. The available bandwidth for the millimeter wave spectrum is 252 GHz [2]. The anticipated scarcity of bandwidth in the currently used microwave bands is due to the fact that the network will need to supply coverage to over 50 billion devices by year 2020 [2]. The use of millimeter wave frequencies has some weaknesses. One is that the range is limited due to electromagnetic signal spreading loss increasing with frequency. Also, various materials, such as human skin, clothing and plaster have shown to be effective attenuators of millimeter wave signals. Next, the short coherence time at high frequencies causes rapid variations of the channel. Finally, higher frequency signals entering a digital signal processor require a higher sampling rate thus causing more power consumption.

1.2.1 Urban Measurements in New York City

The measurements conducted in NYC show that millimeter wave systems in the future can take advantage of reflections and scattering to operate in ranges of 100 to 200 meters. This range surpasses previous expectations and simulation results [2]. In addition, capacity estimates show that millimeter wave systems can provide much higher data rates than the current outdoor 4G LTE networks. The bandwidth of 4G is 20 MHz [5] whereas the available bandwidth for millimeter wave systems is 252 GHz [7]. The contributions of

[2] described above are important because companies can use this information to solve future network capacity and performance issues. New measurements surveyed in the paper are unique since they were the first to take advantage of the surrounding urban environment at 28 and 73 GHz by getting the majority of signal power from building reflections [2].

The paper develops statistical models from measured data to evaluate the channel capacity. Line of sight (LOS) and non-line of sight (NLOS) path loss models were developed, and these can be used to estimate potential link ranges for 28 and 73 GHz systems. Measured results show that with moderate power levels (provide example number here) and directional antennas, signals can still be received up to 200 meters. To further characterize the channel, the angle of arrival and power delay profiles were also calculated. The angle of arrival is a measurement that determines the direction of a received signal along with signal power. The power delay profile gives the signal intensity as a function of time delay, and is approximately a "power version" of the channel impulse response. Finally, signal to interference plus noise ratio (SINR) and rate distributions indicate that millimeter wave systems provide much higher capacity than today's 4G network. The rate distribution shows the probability that a system provides a certain throughput in mega bits per second (Mbps). When modeling the channel at 28 and 73 GHz, the paper used a standard linear fit method based on measured data. The line that runs through the data is the average and has a slope of β and is centered on the data that has a standard deviation of σ. β is unitless and σ is in dB. For the 28 GHz data, β and σ were found to be 2.97 and 8.7 dB respectively. At 73 GHz parameters β and σ were 2.45 and 8 dB.

To accurately estimate the channel capacity and performance, more millimeter wave measurements will have to be made. With more data available, issues can be

identified through more experimentation and analysis. In addition, [2] mentions design issues that will need to be considered for 5G. One challenge is that new synchronization and broadcast signals will need to be designed for initial cell search. Other challenges mentioned include supporting new multiple access schemes, relays or repeaters and dealing with higher Doppler spreading.

1.2.2 Indoor 60 GHz Measurements

To increase data rates and reduce attenuation, 60 GHz antennas with focused and electrically steerable beams were proposed by University of Wisconsin-Madison in 2015 [6]. In addition, a platform that can reconfigure its carrier frequency, output power and type of waveform was implemented by a software defined measurement device. It was shown that 60 GHz signals are vulnerable to human blockage and device movement. This is a result of measurements that quantify attenuation due to humans within LOS of the transmitter [6]. It is also a result of simulations that show that constant re-beamforming is needed when the receiver moves [6]. However, these issues can be overcome by beam switching, spatial reuse between beams, and link recovery methods.

The main contribution of [6] is the description of the first software-radio device that operates in the 60 GHz band. Also, the methods proposed in this paper are important contributions since they are the first to address modern practical issues concerning millimeter wave networking. These issues include human blockage and antenna movement. The data shown throughout the paper is used to support its arguments for dealing with shadowing by humans and antenna movement. The average shadowing attenuation was 36 dB. For example, results in [6] show that throughput increases and

latency decreases when the proposed beam steering algorithm is used. In particular, Figure 20 in [6] shows that a signal can still be received as a result of human blockage and device movement as well as differences between the two effects. More issues left open are 60 GHz band software defined measurements for other channels such as outdoor rural or urban environments. In addition, [6] mentions the design of new protocols that address future challenges and opportunities such as the sensitivity of highly directional links. This work used the line of sight log-distance path loss model, and found the path loss exponent (slope) to be 1.6 and shadowing factor standard deviation of 1.8 dB.

CHAPTER 2

BASIC PHYSICS, PRINCIPLES AND PROPAGATION MODELS

2.1 Introduction

When signals travel from a transmit antenna to a receive antenna, they travel through what is known as the channel. The channel has a significant role in the performance of the system and is an essential part to the design and implementation of wireless communication systems. As the transmitted signal travels, its power level decreases as it moves from a source to a distant observer or receiver. Depending on the paths the signal takes to reach the receiver, the signal may also incur distortion. The receiver or observing device could be mounted in a wide variety of places, such as on a mobile or cellular phone, a ground vehicle on a tarmac or aircraft.

The path loss quantifies the decrease in transmitted signal power as it propagates in space [9]. To deploy and design a wireless system, such as one for ground-ground communication at airports, an appropriate path loss model is very useful. Path loss modeling is a fundamental task in wireless system design. In particular, the path loss model developed for a certain channel can be used to calculate the link budget of the system to estimate the maximum distance range over which the system can operate.

In this chapter, the basic physics and principles of wireless signal propagation and measurement are discussed. These physical principles include reflection, scattering and diffraction. The effect of receiver noise and noise figure will also be discussed. In addition, this chapter will review some of the common propagation models that were previously developed and commonly used to design wireless systems.

2.2 Basic Physics and Principles

Reflection: When an electromagnetic wave travels from one medium (material such as air or water) to another medium, at the interface that wave may get directed in a different direction [2]. This phenomenon is known as reflection. In wireless communications, a physical phenomenon is classified as a reflection when the medium or object that the signal encounters is relatively large compared to the wavelength of the signal. The extent to which the wave gets reflected depends on the frequency, dielectric constant (or index of refraction), permeability, and conductivity of the two media, and the incident angle of the electromagnetic signal.

Refraction: In addition to reflection, the electromagnetic wave may propagate through an interface between two materials with different electrical properties, or a material with a continuously variable dielectric constant. This phenomenon is known as refraction [4]. As with reflection, the angle at which the wave propagates through, as well as the portion of the signal power that propagates through the medium or along the interface also depends on the electric and magnetic properties of the signal. It also depends on the frequency of the electromagnetic wave.

Scattering: This physical event occurs when the wavelength of the incident signal is near the same size or larger than the object with which it makes contact [2]. The frequency that is being used in this paper is 31 GHz. This frequency is in the millimeter wave region of the electromagnetic spectrum. The relationship between the frequency f and wavelength λ of an electromagnetic signal is given by $c = \lambda f$, where c is equal to 3×10^8 meters/second (speed of light). This yields a free-space wavelength of 9.7 mm for 31 GHz. Due to the very small wavelength, most of the physical phenomena encountered during propagation will likely be reflections more often than scattering. However, scattering is still possible, and must still be considered. Because of this possible scattering and reflections, multiple copies of the transmitted signal generally can arrive at the receiver. They may constructively or destructively interfere. Constructive interference happens when peaks and troughs of one signal align with those of another. Destructive interference (often termed multipath or small-scale fading) happens when the peaks and troughs of one wave tend to cancel another.

Diffraction: This phenomena occurs when the electromagnetic signal meets another object that has sharp edges or corners [2]. An example of materials that could cause diffraction are wall corners in a hallway, rectangular pillars, and stair cases. Even when there is no clear path between the transmitter and receiver, the signal can still be in effect "bent" around corners or objects as a result of this physical mechanism. When the signal leaves a source and meets the receiver or observing device when there is no clear path, this is known as shadowing, sometimes also termed blockage, or obstruction.

Receiver Noise and Noise Figure: The sensitivity or threshold of a receiver is an important property that determines the performance of a wireless communication link. The threshold is the lowest required signal strength for a given performance. Thermal disturbances of electrons cause the usually dominant component of noise at the receiver. This disturbance is likened to Brownian motion. The basic model for this noise is a Gaussian amplitude distribution [4]. It is spectrally "white," meaning its power spectral density is constant for all frequencies. Noise has a power spectral density typically denoted $N_o/2$ for the entire frequency range. In probabilistic terms, this thermal noise is also independent of the wireless signal being received. The thermal noise at the receiver is additive. This thermal noise is typically designated additive Gaussian white noise (AWGN) [4].

The power of thermal noise found at the receiver is given theoretically as follows:

$$N = kT_oB, \tag{2.1}$$

where,

N = the power of the thermal noise at the receiver, in watts

k = Boltzman's constant = 1.38 x 10^{-23} J/K

T_o = the standard noise or room temperature which is usually given as 290 K

B = bandwidth of the receiver, in Hz.

In practice, different components present add noise to this thermal noise power at the receiver. This makes the actual noise greater than that predicted solely by (2.1). Components that make up the receiver include amplifiers, filters, cables, etc. Therefore, it is most accurate to determine the thermal noise power by characterizing it by an *effective*

temperature or noise figure. Hence, a more practical equation for determining thermal noise power can be given as

$$N = kT_oBF\ , F = (1 + T_e/T_O), \tag{2.2}$$

where,

F = Noise figure of the receiving device (dimensionless)

T_e = The equivalent noise temperature of the receiver, in K.

To consider the noise at the receiver when estimating a link budget, it is more efficient to calculate the noise at the receiver in decibels (dB). The equation that computes the actual noise power of the receiver in decibels relative to a specific power level (dBm, or dB relative to 1 mW in this case) is given as follows:

$$N(dBm) = -174\ dBm/Hz\ + 10\log(B) + F_{dB}\ . \tag{2.3}$$

The -174 factor is the constant theoretical value of the power spectral density in dBm/Hz for T=290 K.

2.2 Propagation Modeling

The purpose of modeling propagation is to determine the probability that the performance of the wireless communication system satisfies requirements and provides good quality of service [2]. Path loss modeling is a key component of propagation modeling, used in planning or designing a communication network. The effectiveness and applicability of the path loss model can affect the price and performance of the network. In

terms of communication network design, the main purpose of modeling the wireless channel is to estimate the received signal strength over a range of link distances. Wideband channel models are also used to estimate parameters that are useful in signal design to avoid or compensate for distortion.

One can predict the received signal strength if the amount of attenuation and transmit power are known. The path loss is just the difference in dB between the transmitted signal power and received signal power (or if in linear units, the ratio of transmit to receive power). Path loss can "encapsulate" reduction of signal strength due to all phenomena such as reflections, scattering, diffraction, and spatial spreading. Path loss also depends on the type of environment, frequency, and antenna heights. Common environment types are urban, rural and suburban. Depending on the application of the communication system and the variables given previously, companies start the design process by picking the model that best fits the scenario.

2.2.1 Common Propagation Models

There are several common propagation models used to predict path loss. These models are used by researchers and engineers to compare and evaluate empirical results. What follows is a survey of basic propagation models often used in wireless engineering and applications.

Free Space Path Loss Model

The free space path loss (FSPL) model does not include reflections, scattering, diffraction or any other influence on the signal caused by objects. This means that the free space model assumes a clear line of sight (LOS) between the transmitter and the receiver. The loss is normally expressed in dB. Common systems that follow this model are satellite and microwave point-to-point communications systems. This is because in those scenarios, the transmitter and receiver are far away from any obstacles, allowing direct point to point communication. The received signal power can be found using the Friis equation [2], given by

$$P_{Rx} = P_{Tx} \frac{g_T g_R}{\left(\frac{4\pi d}{\lambda}\right)^2} \tag{2.4}$$

where,

P_{Rx} –power received at distance d,

P_{Tx} –transmit power,

g_t - transmitting antenna gain,

g_r - receiving antenna gain,

λ –wavelength,

d –distance from the transmitter to receiver.

To express the attenuation in decibels (dB) we use

$$L_{dB} = 10\log\left(\frac{P_{Tx}}{P_{Rx}}\right), \tag{2.5}$$

which then results in

$$L_{dB} = 10\log(\frac{(4\pi d/\lambda)^2}{g_r g_t}). \quad (2.6)$$

From the above the total loss is given by

$$L_{dB} = 20\log\left(\frac{4\pi d}{\lambda}\right) - G_R - G_T. \quad (2.7)$$

To calculate the link budget using this attenuation model, the equation is given by,

$$P_{r(dB)} = P_{T(dB)} - L_{dB} \quad (2.8)$$

which finally gives the link budget equation,

$$P_{r(dB)} = P_{T(dB)} - 20\log\left(\frac{4\pi d}{\lambda}\right) + G_R + G_T. \quad (2.9)$$

This is the fundamental equation used to derive the received signal power at some distance assuming line of sight free space path loss and antenna parameters. The free space path loss is the 2nd term in (2.9). In chapter 5, where the analysis of our experiments is described, noise at the receiver will be considered in the link budget equation. Cable losses will also need to be considered for the analysis.

The Two Ray Model

Methods of modeling propagation based on the signal traveling multiple paths are needed because physical phenomena such as reflections, scattering, diffraction and other phenomena caused by objects in the environment affect signal attenuation. The free space model is not accurate enough to estimate the received power as the communication link environment becomes more dense with objects or humans [4]. Multipath models make calculations of the path loss based on geometric paths that the signal takes from the

transmitter to receiver. These geometric paths can include both line of sight and straight line paths reflecting from the ground, walls and other objects. A basic multipath model is the two ray model. This model only considers a ground reflection and the line of sight path. This model is used for applications for any communication link that involves using a transmitter and receiver near earth with minimal obstacles.

The simplified equation [5] used to predict the attenuation in a two-ray link case is given by

$$L_{2-ray} = \frac{(4\pi d/\lambda)^2}{4sin^2(2\pi h_t h_r/\lambda d)}, \tag{2.10}$$

where,

h_r –height of the receiver antenna,

h_t –transmitter antenna height,

d- distance from the transmitter to receiver,

λ - wavelength.

If d is very large such that $d >> h_t$ and h_r, the small argument approximation can be used for the sine term, and the equation becomes

$$L_{2-ray,large\ d} = \frac{d^4}{h_t^2 h_r^2}, \tag{2.11}$$

which, in decibels (dB), becomes

$$L_{2-ray}(dB) = 40\log(d) - 20\log(h_t) - 20\log(h_r) \tag{2.12}$$

Like all models, the two ray model has some weaknesses. The first weakness is that it assumes that the ground is completely flat. Any sharp edges or irregularities on the ground may cause scattering, reflection or even diffraction effects. A second weakness is that in a practical application or system, obstacles are likely, hence this model is only useful

in areas where the transmitter and receiver line of sight path has no nearby objects. The approximate model also assumes that the antenna gains (at both Tx and Rx) are identical for the LOS path and the reflection; this approximation generally improves as distance increases. Finally, the assumption $d>>h_t, h_r$ yields a small angle of incidence for the reflection, that enables approximation of the reflection coefficient by unity. Violation of any of these assumptions requires use of a more accurate equation than (2.10).

Empirical Channel Models

Path loss models that estimate attenuation or propagation loss analytically tend to be accurate when applied in settings where appropriate. This is because they are based on the physical laws of electromagnetic propagation [6] for simplified conditions. The analytical models often cannot consider all influences or phenomena that effect propagation, and if they attempt to do so, they tend to be very complex because they require large amounts of information. This information includes details of all geometric information from the environment and objects that block the paths of propagation. This information also includes the electrical parameters—permittivity, permeability, and conductivity—of all objects in the environment. Due this large amount of data, analytical models require large amounts of computational power and effort. For a wide area or environment with many obstacles that are static or moving, the computational power required to use an analytical model may significantly surpass the limits of current computers. Even if one has powerful computers, accurate estimates of material electrical parameters are often unavailable.

With this in mind, it should be noted that accuracy may be sacrificed for ease of computation. That is usually done for the sake of cost and practicality. To do this

effectively so that the model is sufficiently accurate, a model based on wireless measurements taken in the field is often considered. Models based on real data are called empirical propagation models. In order to create such a model, an extensive campaign of wireless propagation or path loss measurements should be made. These models also often represent various model quantities (parameters) statistically rather than deterministically.

An empirical model best satisfies the wireless design or application if the environment where the measurements were taken is similar to the type of place where the wireless system will be deployed. The advantage of this type of model is that is considers all parameters concerning propagation such as antenna gains and positions. However, in order for this model to likely satisfy its application, correction factors must often be added. Correction factors account for any possible errors or uncertainties in the measurements. Some of the most common empirical models based on measured data are discussed next.

The Okumura-Hata Model

Okumura, Ohmori, Kawano and Fukuda made extensive wireless measurements in 1968. These measurements took place in several different environments throughout Tokyo, Japan. From these measurements, they developed a large series of curves of field strength vs. distance. This group of curves gave median attenuation relative to free space path loss. However, the empirical plots in the 1968 report were not convenient to use. For this reason, Hata developed equations to describe the data in 1980. These expressions were developed in the following closed forms, [5]:

$$L_{50} = \begin{cases} A + Blog(d), & for\ urban\ area \\ A + Blog(d) - C, & for\ suburban\ area, \\ A + Blog(d) - D, & for\ an\ open\ area \end{cases} \tag{2.13}$$

where,

$A = 69.55 + 26.16\log(f_c) - 13.82\log(h_b) - a(h_m)$,

$B = 44.9 - 6.55\log(h_b)$,

$C = 5.4 + 2[\log(f_c/28)]^2$,

$D = 40.94 + 4.78[\log(f_c)]^2 - 18.33\log(f_c)$,

and

$$a(h_m) = \begin{cases} (1.1\log(f_c) - 0.7)h_m - 1.56\log(f_c) + 0.8, med\ or\ small\ city \\ 8.28[\log(1.54h_m)]^2 - 1.1, large\ city, f_c \leq 200MHz \\ 3.2[\log(11.75h_m)]^2 - 4.97, large\ city, f_c \geq 400MHz \end{cases} . \quad (2.14)$$

This model depends on the antenna heights of the transmitter and receiver, correction factors, the environment and frequency. These models showed that when antenna height increased, the path loss decreased. They also showed that path loss increases with frequency, as expected. The Hata model approximates the model developed in the Okumura paper accurately for distances link distances greater than 1000 m.

The model is designed for frequencies that range from 150-1500 MHz. This model and associated frequency range make it only practical for cellular systems of the first and second generations. Even though the model was created decades ago, it is still used and has often proved to be better than modern models. However, systems that are designed to use higher frequency bands, such as microwave and millimeter wave bands, will need new models to be developed.

Log Distance Models

At any specific location or distance, the channel attenuation can be broken into three fundamental parts: shadowing (which is typically modeled as random and log normal), small scale fading due to multipath propagation, and spreading loss due to the distance between the transmitter and receiver. A log-distance path loss model estimates the path loss at a given link distance with respect to some reference distance. The reference distance chosen depends on the environment in which the system will be deployed, as well as the far field distance of the antennas. A general expression for the log distance path loss model, in dB, is as follows, [5]:

$$PL(d) = A + 10nlog(d/d_0) + X, \tag{2.15}$$

where,

A- intercept at distance d_0, in decibels,

n- path loss exponent (dimensionless),

X- Gaussian random variable in dB,

d- link distance between the transmitter and receiver,

d_0- chosen reference distance.

The variable A is a factor that fits the measured data by taking into account the antenna gains, known transmit power, transmission cable losses and the received power at the chosen reference distance. The path loss exponent n depends on the environment and is determined using a statistical analysis of measured path loss data. The variable X is a random variable that quantifies the goodness of fit of the line expressed by the first two terms. Typically X is modeled as a Gaussian random variable with mean zero. The variance

of this value is found by using the least squares curve fitting method on the set of measured data. Again, since the reference distance depends on the environment, a different value of d_0 can be chosen for each application. Since this thesis focuses on measurements made at a local airport, we will use the airport surface and indoor environments as an example. The total distance of the outdoor airport surface is on the order of a few hundred meters, so a reference distance from 1 to 5 meters will suffice. However, the total length of the indoor airport environment at the main building is on the order of tens of meters, so the reference distance chosen should be on the order of one meter.

Lee Propagation Model

Another relatively popular propagation path loss model is the Lee propagation model. The main components of this model are the influences of the signal due to natural terrain and effects caused by man-made objects or structures. The band of frequencies that this model uses to derive expressions range from 900 MHz to 2 GHz [9]. Several different environment types are considered. These include urban areas (from measurements in Newark and Philadelphia) as well as open and suburban areas. The model depends on distance, antenna heights, transmit power and the frequency of the signal. The Lee propagation model follows this expression, in dB, [7]:

$$L_{Lee}(dB) = L_o + mlog\left(\frac{d}{d_o}\right) - 15\log\left(\frac{h_t}{h_{t0}}\right) - 10\log(\frac{h_r}{h_{r0}}), \qquad (2.16)$$

where,

$L_{Lee}(dB)$ - path loss at some reference distance in dB,

m – slope (dB/decade),

d – link distance from transmitter to receiver (m),

d_0 - reference distance (m),

h_t - transmitter antenna height (m),

h_{t0} - transmitter antenna reference height (m),

h_r - receiver antenna height (m),

h_{r0} - receiver antenna reference height (m).

CHAPTER 3

PRE-TEST MEASUREMENTS

3.1 Battery Test

Before any measurements could take place at the Owens Field airport, equipment was tested in the lab. It was anticipated that the receiver, the signal and spectrum analyzer (SSA), would need to be connected to a DC source at least part of the time. Thus, a test for the equipment's powering duration from a battery was conducted. A 12V marine battery was connected to a 1500 watt inverter that changed the DC power to 60 Hz AC power. The inverter was then connected to the SSA.

The vector signal generator (VSG), which is our transmitter, was connected to an AC power outlet nearby; see Fig 3.1. The VSG was set to send a wide band signal with a bandwidth of 600 MHz and maximum power at 0 dBm to test the maximum capability of the receiver. This signal was sent from the VSG to the SSA via cable. The time it took for the battery to discharge to 10% level while connected to the SSA was recorded. Once the battery could not provide charge and the time was recorded, the battery was recharged until it reached a maximum of 80 percent. Then the process was repeated for each experiment. After several test runs, it was concluded that the battery provides power for this set of equipment for at least 1 hour and 30 minutes.

Figure 3.1 Rohde and Schwarz equipment on desk.

3.2 Outdoor 31 GHz Test Measurement

Test measurements were conducted in and near the Swearingen building before going to the airport, to ensure the equipment list was complete and measurement procedures were defined. A signal with a frequency of 5 GHz and a power level 0 dBm was sent from a vector signal generator. The VSG used was the Keysight, model N5182A MXG. This signal was sent to an RF up converter to shift the signal to 31 GHz. It was then sent to an amplifier, yielding an output power level of 35 dBm. The upconverter was a Microwave Dynamics model LO-MIX301-2832 and the amplifier was a model AP2832-25 made by the same company. The final signal was then transmitted by a horn antenna

with 10 dBi gain with azimuth and half power beam widths of 54.4°. At the receiver, the same model of antenna was used and it was connected to the R&S signal and spectrum analyzer (SSA). The analyzer was a model FSW26/FSW43 made by Rohde & Schwarz.

Both hardware sets were placed on carts with wheels for easy movement. In addition, this allowed both antennas to be easily aligned at the same height. Both antennas had identical heights of 1 meter relative to the ground. On the receiving end, the antenna was placed on a hand made antenna mount so that it would not move unintentionally. It was also made to allow the antenna to be rotated manually to change the polarization of the signal for measurements with different polarization settings.

The test measurement was conducted outdoors on the Assembly Street side of the Swearingen Engineering Center Building at The University of South Carolina in Columbia, South Carolina. Testing was done in the parking lot next to the building during a clear afternoon. Both the transmitter and receiver were connected to an indoor wall power outlet using a series of extension cables and a surge protector. The length of the cables enabled the receiver to move more than 30 m away from the transmitter. This eliminated the need for using the DC power source.

There were vehicles and metal signs nearby that likely interacted with the transmitted signal via scattering, reflection or diffraction; see Fig. 3.2. The concrete ground could also yield a multipath component. A reference power level was measured by placing the receiver 2 m from the transmitter. At this distance, both co- and cross-polarization reference measurements were made; co-polarized denotes vertical for both transmitter and receiver.

Cross polarization measurements were done because during a real world application, the antenna may move to different positions, and we are often interested in cross-polarized levels relative to co-polarized levels. Measurements were taken every 2 m. All measurements were taken in the line of sight (LOS) setting such that nothing blocked the path between transmitter and receiver.

This entire procedure was done to estimate path loss versuss distance for both co- and cross-polarization antenna arrangements. To compute path loss, the cable losses, antenna gains, and transmit power are used. Cable losses were 5 dB each, antenna gains are 10 dB, and the transmit power was 25 dBm.. Using these values, the path loss in dB is computed from the link budget as

$$P_{r(dBm)} = P_{T(dBm)} - L_{cables} + G_R + G_T + -L_{chann} \quad , \tag{3.1}$$

where P_T is the transmit power at the amplifier output, L_{cables} is the sum of Tx and Rx cable losses, G_R and G_T are Rx and Tx antenna gains, respectively, and $L_{channel}$ is the path loss we estimated.

As expected, the power level on average decreases with increasing distance. The results for the co and cross polarized 31 GHz measurements are as shown in Figures 3.3 and 3.4. In addition as the receiver gets further away there are slightly higher power values in certain areas due to multipath scattering (constructive interference) from cars and the ground.

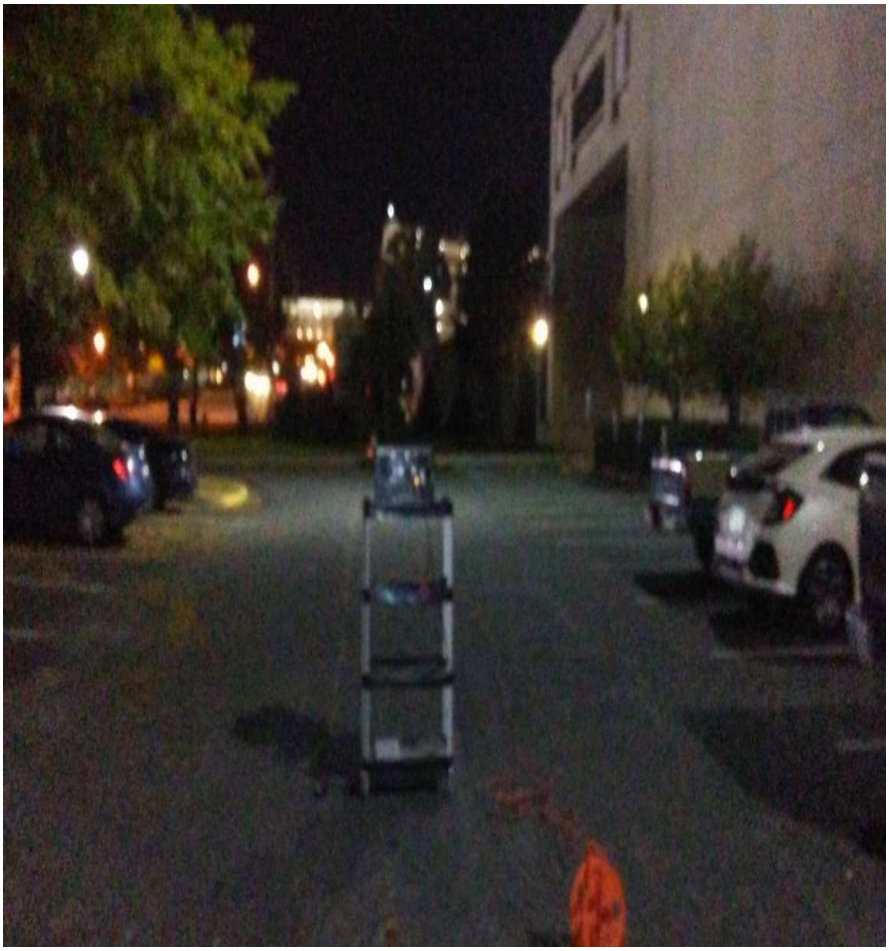

Figure 3.2 Outdoor receiver setup in Swearingen Parking Lot.

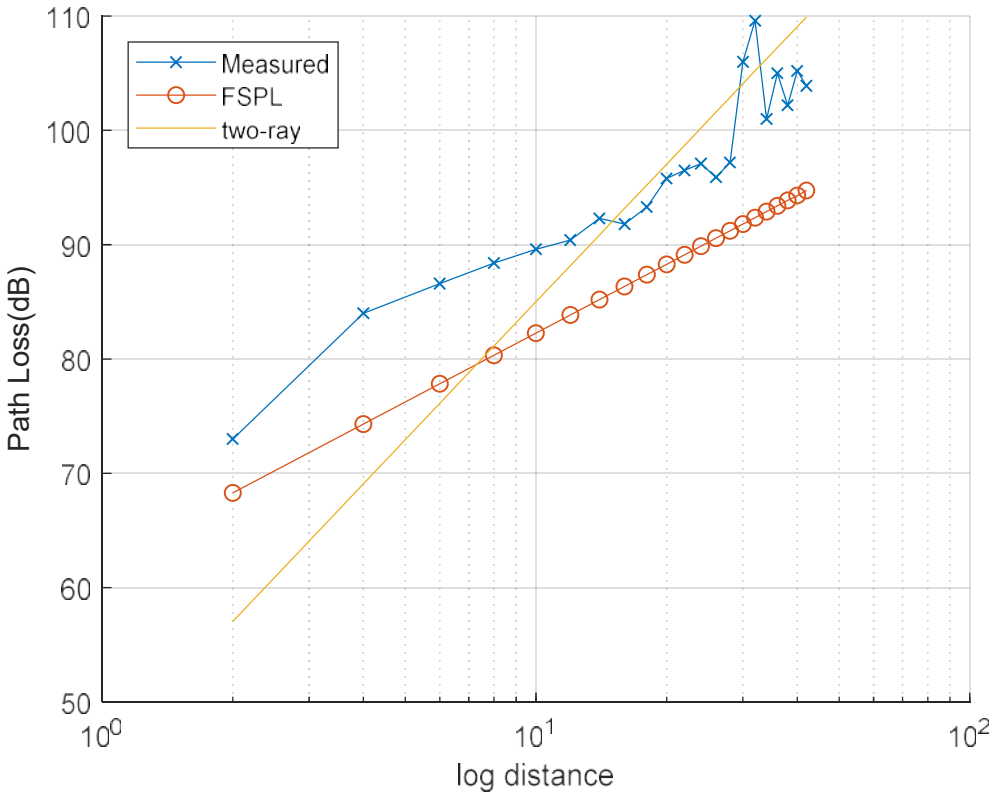

Figure 3.3. Path loss in dB vs. logarithm of distance in meters, for the co polarized measurements in the Swearingen parking lot, for frequency 31 GHz. Free-space and simplified two-ray path losses also shown.

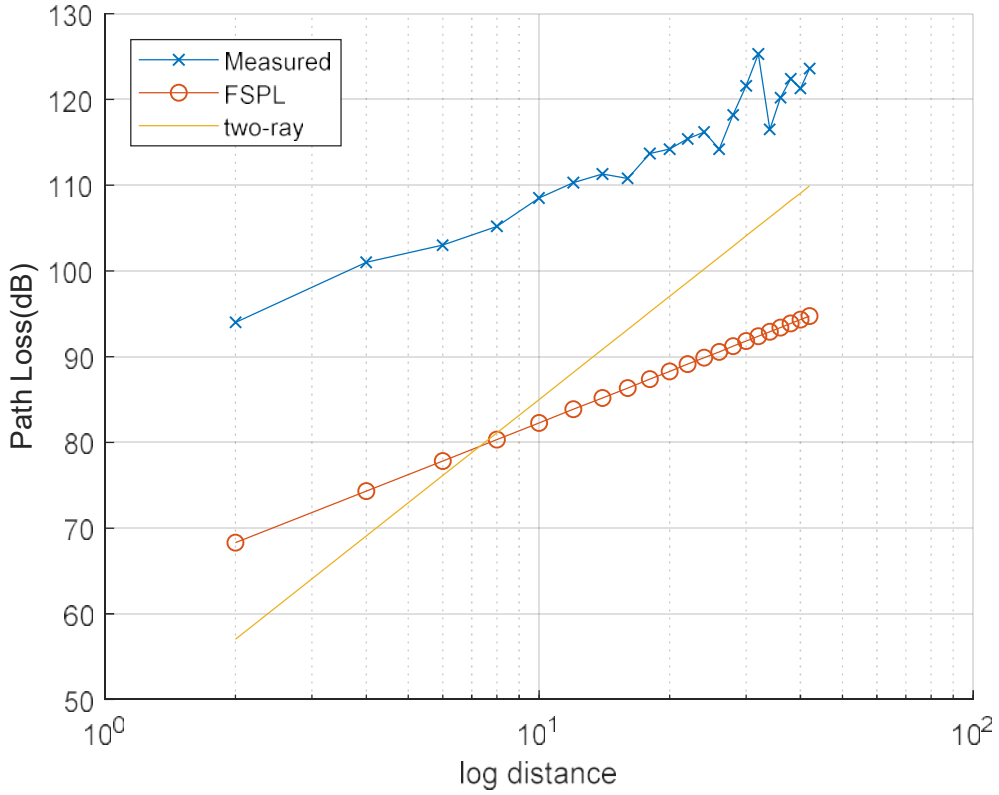

Figure 3.4 Path loss in dB vs. logarithm of distance in meters, for the cross polarized measurements in the Swearingen parking lot, for frequency 31 GHz. Free-space and simplified two-ray path losses also shown.

As expected, the path loss for the cross polarization measurements is larger than that of the co polarized measurements because of the polarization mismatch. Path loss is also larger than that of free space by approximately 6-10 dB for the co-polarized case. This is likely due to insufficient averaging over small scale fading, and an incorrect calibration by the author.

3.3 Indoor Simultaneous 5 GHz and 31 GHz Test Measurements

Additional test measurements were conducted indoors in the hallway near the Wireless Science and Engineering Lab (room 3D-41) on the third floor of Swearingen Engineering Center. Again, the conditions were LOS so that nothing blocked the path between transmitter and receiver. On the transmitter side, the vector signal generator was set to output RF signals to both available ports. The vector signal generator used was the same as described in the prior section. One port was connected to an omni directional 5 GHz antenna. The antenna was a L-COM HGV-4958-06U with gain of 6 dBi. This antenna was connected to the signal generator with a cable and mounted on a custom made antenna mount that stood approximately a meter tall. The other VSG port was connected to the 31 GHz upconverter via cable. All RF components on the 31 GHz transmitter side were also attached to a custom made mount. The upconverter was a Microwave Dynamics model LO-MIX301-2832. This upconverter took the 5 GHz input and shifted it into a 31 GHz center frequency. The signal then entered an amplifier using another cable. The amplifier was the Microwave Dynamics model AP2832-25. This amplifier output power level was approximately 25 dBm. Finally, the amplified signal entered the 31 GHz antenna. The antenna was a Pasternack model pe9850/2f-10, with gain of 10 dBi and half power beam width 54.4^{o}.

At the receiver the 31 GHz signals were captured by another Pasternack antenna identical to the transmitting antenna. The receiver antenna was directly connected to a signal spectrum analyzer. This analyzer was a Rohde and Schwarz FSW 46. For the 5 GHz signals, the receiver antenna was identical to the transmitting omni directional antenna made by L-Com mentioned previously. However a different signal analyzer was used for

the 5 GHz signals. This spectrum analyzer was a portable Agilent HP CertiPRIME N9344C. Both transmitter and receiver set ups were powered by wall outlets along the hall way.

After connecting all components, a reference measurement was made with the transmitter and receiver 2 m apart and facing each other. At this distance, three measurements were made by moving the receiver antenna to three points separated by one-half wavelength (at the same height and link distance). These three power measurements are averaged to be used when calculating pathloss. The three-point measurement process was repeated every 2 m away from the transmitter until we reached a maximum distance of 26 m. Figures 3.5 and 3.6 below show the path loss for 5 GHz and 31 GHz respectively for the indoor hallway environment on the 3rd floor of Swearingen.

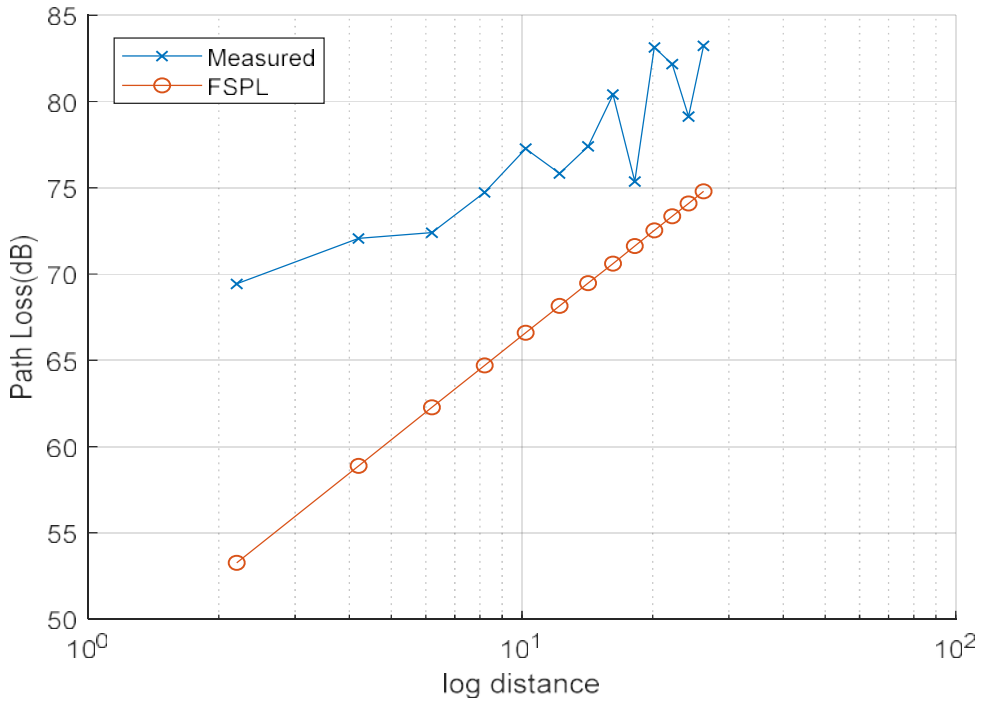

Figure 3.5 Path loss in dB versus logarithm of distance in m for 5 GHz, in 3rd floor D-wing hallway. Free Space path loss (FSPL) also shown.

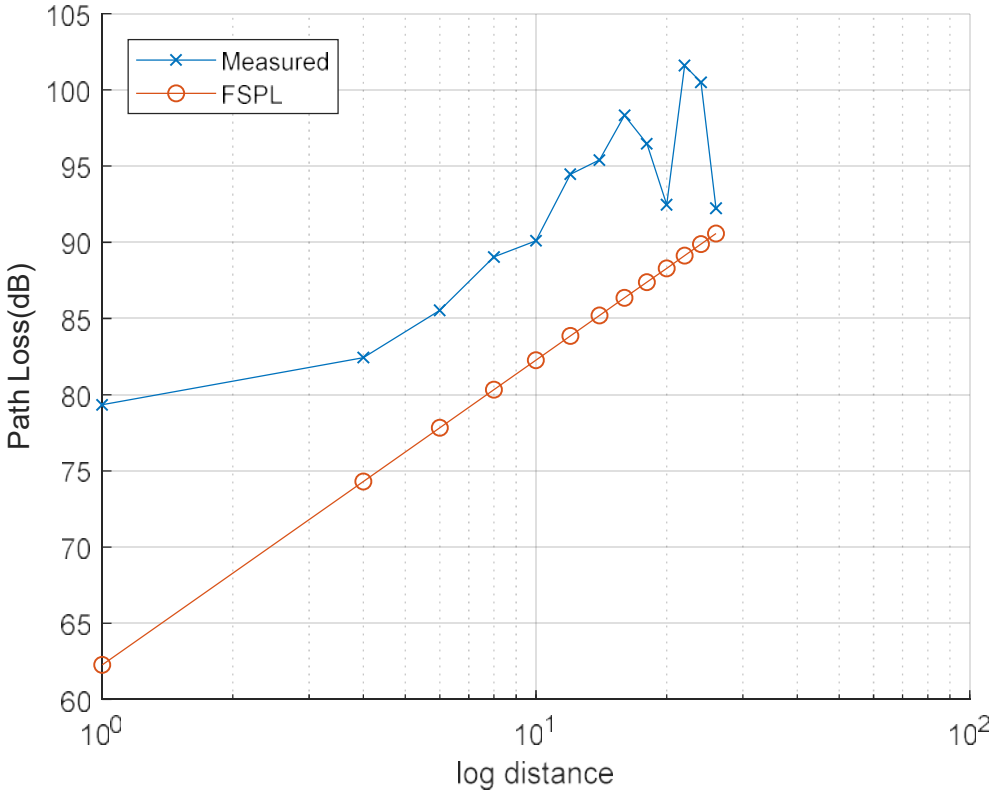

Figure 3.6 Path loss in dB versus logarithm of distance in m for 31 GHz in 3rd floor D-wing hallway

As expected, the 31 GHz signals showed greater path loss than the 5 GHz signals. In addition, all measured loss is greater than free space path loss.

CHAPTER 4

AIRPORT EXPERIMENT SETUP FOR 5 AND 31 GHZ

4.1. Introduction

One of the aims of our NASA project is to evaluate future technologies for improving the safety and efficiency of air traffic management (ATM) systems. Since airports are key components of ATM, we are investigating deployments of new wireless systems at airports, for various applications. In order to ensure such systems meet requirements, a quantitative understanding of the wireless channel over which they operate is essential. This was the purpose of our tests.

We planned to make measurements both indoors and outdoors, but did not complete the outdoor measurements. Hence this thesis reports only on the indoor measurements. The measurements were made at two separate (and non-interfering) frequencies, 5 GHz and 30 GHz. These frequencies are well above any currently used at the Jim Hamilton L B Owens Field Airport for airport operations, and hence did not pose any interference problem. The test procedure broadly consisted of selecting the transmitter location, and transmitting a single sinusoid in each band, to the receiver that was moved about the local area. Indoor test distances were limited to a few tens of meters,. We coordinated with airport personnel to ensure no interference with normal airport operations.

4.2. Test Equipment

The test equipment consisted of two transmitters and two receivers, along with associated antennas, cables, power supplies, and carts for moving the equipment. A list of equipment is provided in Table 1.

Table 4.1 Equipment required for airport channel measurements.

Equipment	**Manufacturer and Model Number**	**Comments**
Signal and Spectrum Analyzer (SSA)	Rohde and Schwarz FSW 46	Receiver for 31 and 5 GHz signals
Spectrum Analyzer	Agilent HP CertiPRIME N9344C	Receiver for 5 GHz signal
Vector Signal Generator (VSG)	Rohde & Schwarz SMW 200A	Generates transmitted signals
Directional Horn Antennas	Pasternack pe9850/2f-10	horn antennas for 31 GHz
Omni Directional Antennas	L-COM HGV-4958-06U	omni directional for 5 GHz
RF Amplifier	Microwave Dynamics AP2832-25	gain 24 dB
Upconverter	Microwave Dynamics LO-MIX301-2832	frequency shifts IF signal up by 26 GHz

Wooden Antenna mount	n/a	Hand made antenna mount that stands 1 m tall
Extension cords	n/a	3, for connection to AC power, ~ 30 m long
Surge protected power strip	n/a	n/a
12 volt marine DC batteries	Duracell Ultra BCI Group 31M Deep Cycle Marine & RV Battery	Provides powers for portable equipment via inverter
1500 Watt power inverter	Tiger Claw 1500W Pure Sine Wave Power Inverter DC-AC	Converts DC power from batteries to AC power for portable equipment
Two carts for transporting equipment	n/a	~ 1 m tall

4.3. Test Procedures

A block diagram of the test configuration is shown in Figure 4.1. Generally, test procedures were largely the same for all test locations, although site specific characteristics

required some adjustments. Four people conducted the tests, two at the transmitter site, and two at the receiver sites.

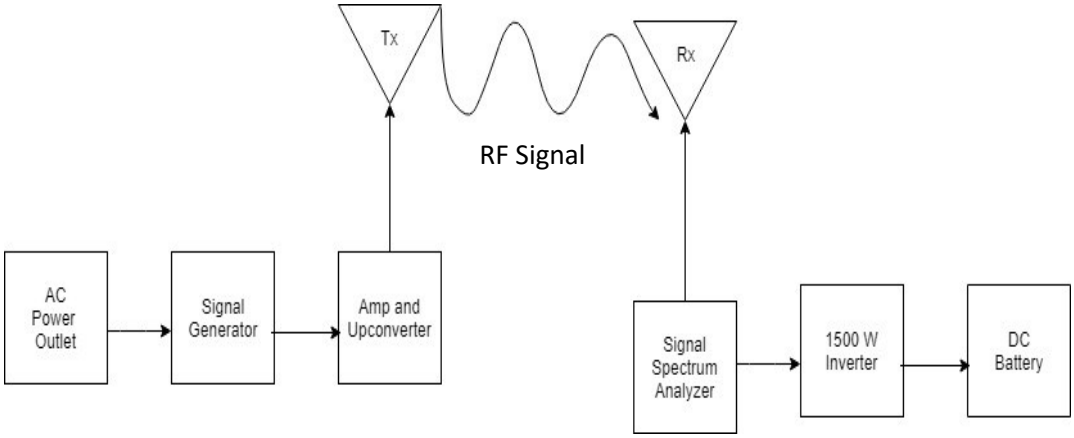

Figure 4.1 Diagram of test configuration showing equipment connections.

A cart with the transmitting antennas on the wooden mount and vector signal generator were placed in several different locations. We did measurements in several locations. Measurements took place inside the terminal building in the main hallway, and in three different rooms; for these measurements, the transmitter was located on the first or second floor.

The receiver was powered by battery for all experiments. We coordinated with airport personnel to ensure no disruption to airport operations, and to maintain personnel and equipment safety. The life of each battery was estimated at approximately 1 hour and 15 mins when powering the R&S receiver.

The transmitters were powered using the available AC outlets inside the Eagle Aviation building for the first two transmitter positions. We did both line of sight (LOS) and non-LOS (NLOS) measurements during this campaign. Before testing, all cable losses

for each of the transceivers (5 GHz and 31 GHz) were measured. The steps of our measurement procedures are as follows:

1. Place cart with transmitters in one of the designated locations
2. Connect VSG to AC power and turn it on, allow for software boot up.
3. Place cart with receivers 1 m away from cart with transmitters.
4. Ensure battery is connected to inverter and inverter is connected to SSA.
5. Power on SSA and allow software boot up.
6. Connect all antennas (Tx and Rx) to required ports via RF cables.
7. Set VSG to transmit a sinusoid at the test frequencies 5 GHz and 31 GHz at maximum power level. Do not turn RF power on until Rx team indicates ready.
8. Set SSA and portable SA to appropriate center frequency, attenuation, resolution bandwidth, and video/display bandwidth.
9. When Rx team ready, instruct Tx team to turn on RF transmit power. Record 1 m power reference values: five (5) for each frequency—all at same link distance—with five points separated by at least one-half wavelength.
10. Move the Rx cart with the receivers and their power supplies away from the transmitter to the next measurement point, at 2 m farther from the Tx. (Note: for NLOS measurements, Rx may not be moved along direct Tx-to-Rx line path.)
11. Take the average of the five samples at each measurement distance to obtain an average value of received power for that distance.
12. Repeat for the other designated areas

CHAPTER 5

AIRPORT MEASUREMENT RESULTS AND ANALYSIS

5.1 31 GHz Measurements and Data Analysis: Terminal Building

The following results pertain to both LOS and NLOS cases. All data was organized in Microsoft Excel® and then placed into MATLAB® for analysis and plotting. Figure 5.1 shows path loss in dB versus the log of distance for the first of three "runs" inside the terminal building. A run is a single measurement path, in which the transmitter is stationary, and the receiver is moved. For Figures 5.1-5.4, all results are for LOS conditions.

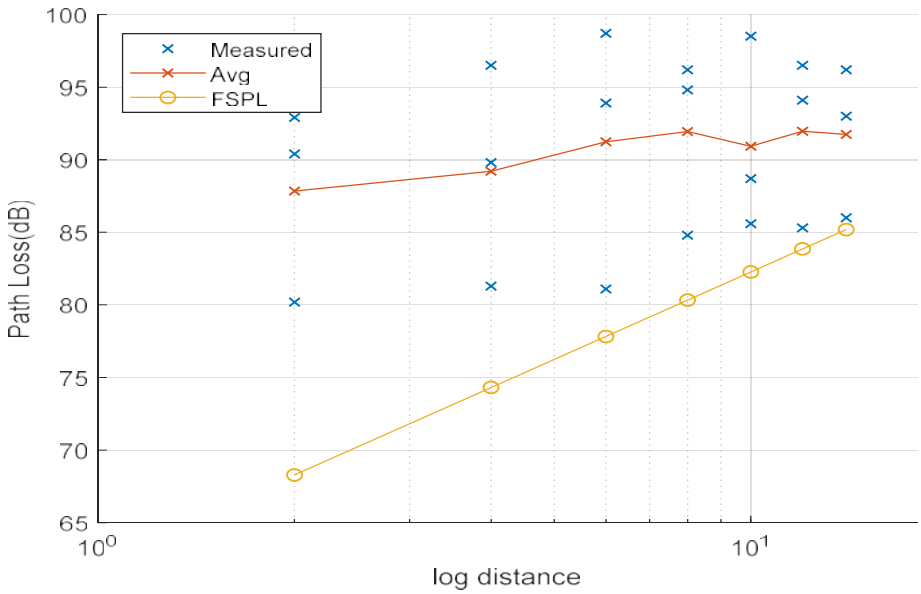

Figure 5.1. Measured, average, and free-space path loss vs. logarithm of distance, CUB Terminal building, 31 GHz, LOS Run #1.

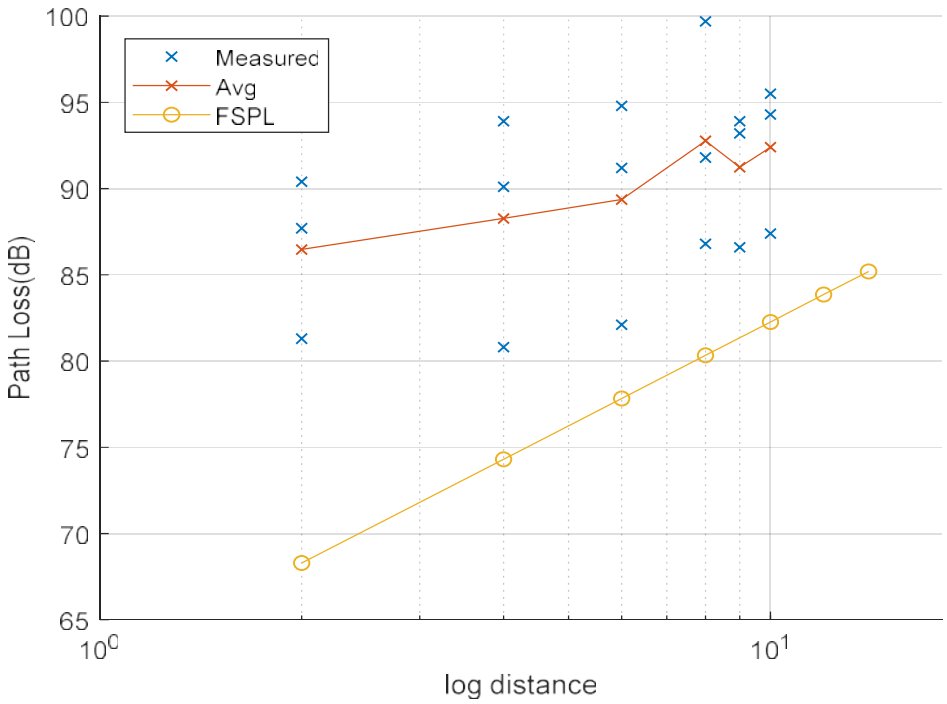

Figure 5.2 Measured, average, and free-space path loss vs. logarithm of distance, CUB Terminal building, 31 GHz, LOS Run #2.

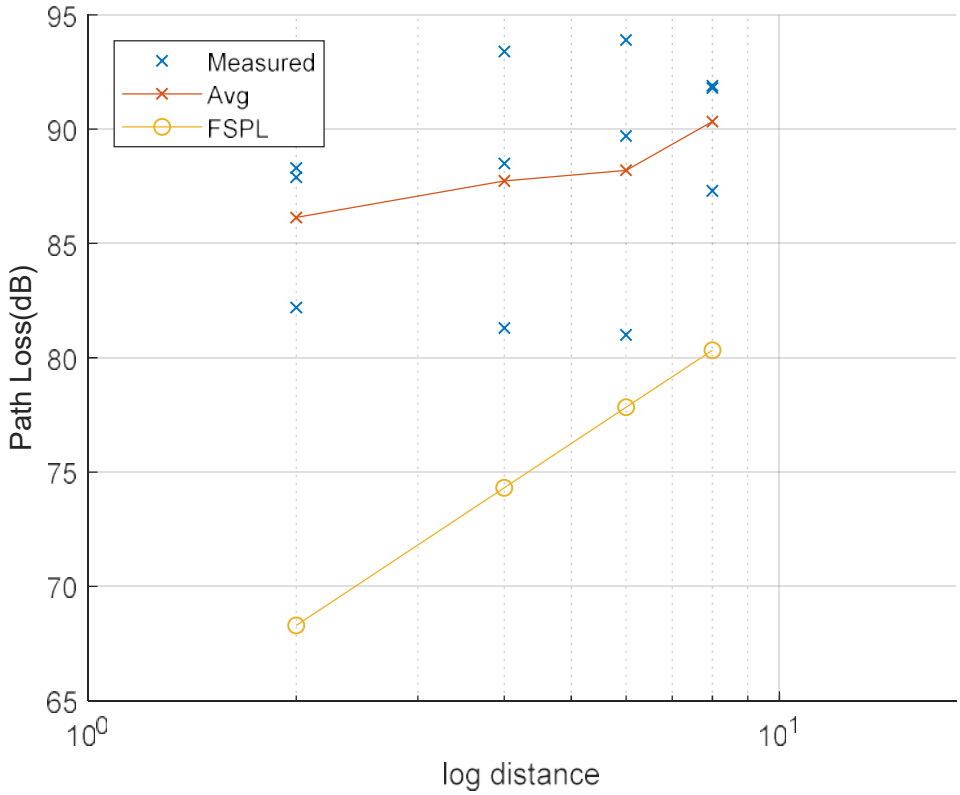

Figure 5.3: Measured, average, and free-space path loss vs. logarithm of distance, CUB Terminal building, 31 GHz, LOS Run #3.

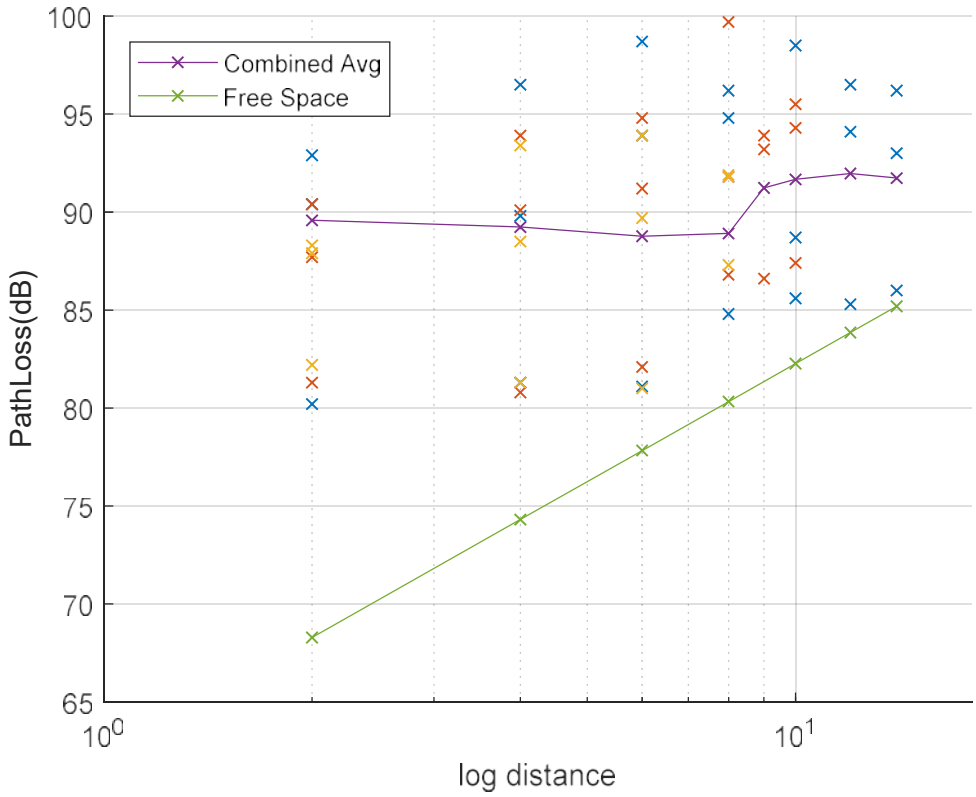

Figure 5.4: Combined average and free-space path loss vs. logarithm of distance, CUB Terminal building, 31 GHz, LOS.

The modeling technique that was implemented to describe the 31 GHz LOS data is known as the close-in free space reference distance (CI) path loss model [2]. Its equation comes in the form

$$\mathrm{PL}^{\mathrm{CI}}(f, d)[\mathrm{dB}] = \mathrm{FSPL}(f, d_0) + 10n \log_{10}\left(\frac{d}{d_0}\right) + X_\sigma^{\mathrm{CI}} \quad , \tag{5.1}$$

for distance $d \geq d_0$, where distances are in meters, d_0=1 m is the reference distance, X_σ^{CI} is a zero mean random variable with standard deviation σ dB, and $FSPL(f, d_0)$ is the free space path loss discussed in Chapter 2. The parameter n is the slope versus $10log(d)$. Variable X is typically modeled as Gaussian.

After LOS measurements were finished, non-line of sight (NLOS) measurements were also taken in different rooms. For these NLOS measurements, the transmitter was placed in two different locations, one on the first and the other on the second floor. The transmitter location for the first floor was the main hall way. When there was a potential for LOS, to ensure that no LOS path was present, the receiving horn antenna was pointed 90^0 away from the direction of the transmitter antenna. Figures 5.5 and 5.6 show the measured, average, least squares (LS) fit to the data, CI model and free space path loss for the NLOS setting in the terminal building. Figure 5.7 shows the same results after combining data from Figures 5.5 and 5.6.

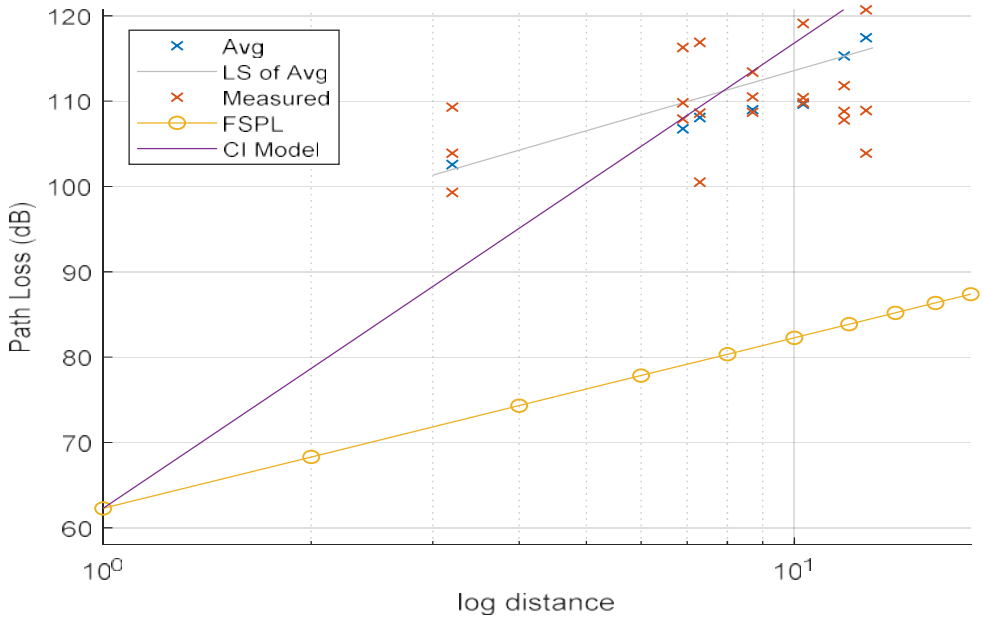

Figure 5.5 CI model, measured path loss, measured average, least squares fit to average, and FSPL vs. logarithm of distance in two rooms in the terminal building at 31 GHz, NLOS.

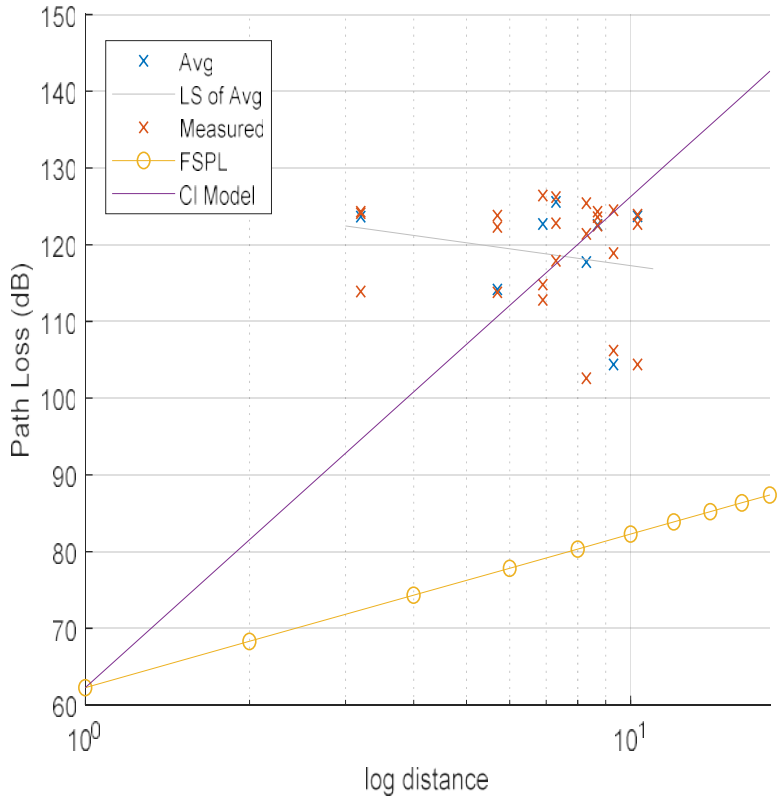

Figure 5.6. CI model, measured path loss, measured average, least squares fit to average, and FSPL vs. logarithm of distance in one room and from upstairs in the terminal building at 31 GHz, NLOS.

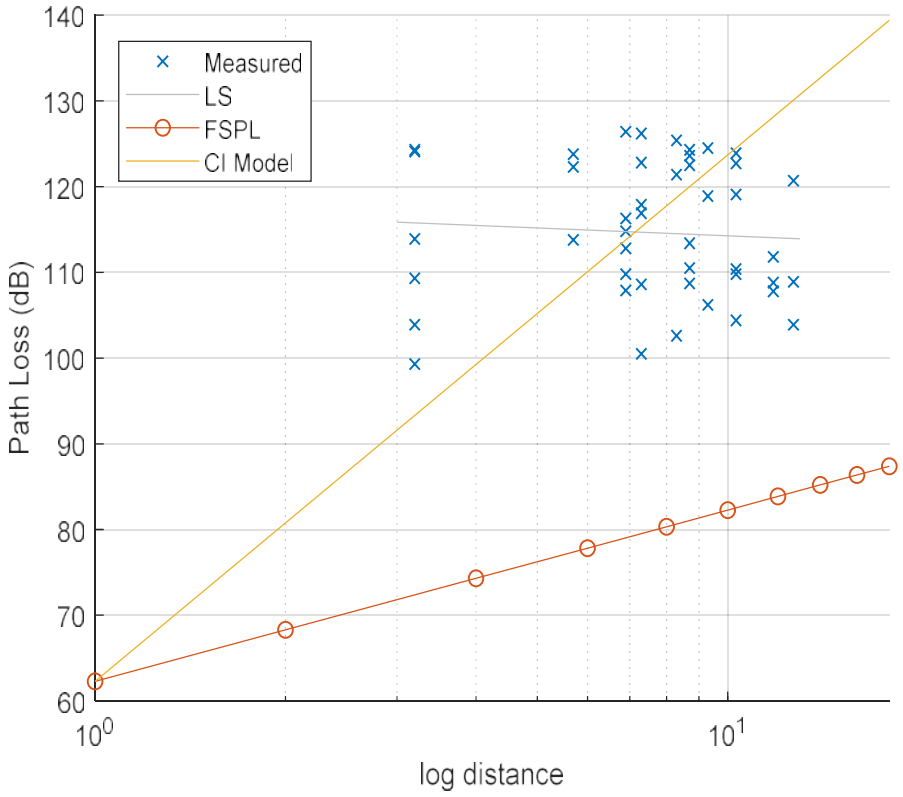

Figure 5.7 CI model, measured path loss, measured average, least squares fit to average, and FSPL vs. logarithm of two previous data sets 31 GHz, NLOS

For LOS data, the average loss is larger than that of free space, although the slope of the LS fits do roughly parallel the free space line. Path loss is larger than that of free space by approximately 10 dB for the co-polarized case. This is likely due to insufficient averaging over small scale fading, and an incorrect calibration by the author. The NLOS path losses are significantly larger than that of free space, as expected. Model results for all terminal building NLOS path loss measurements are listed in Table 5.1

Table 5.1 CI path loss model parameters: standard deviation and path loss exponents of indoor runs, NLOS, terminal building.

Run	**σ**	N
1	5.4518	3.15
2	7.0378	2.84

5.2 31 GHz Measurements and Data Analysis: Maintenance Hangar

A series of measurements were taken inside a maintenance hangar. The measurements were taken in LOS, partial LOS, and NLOS settings.

For the set of measurements inside the maintenance hangar, most of the measurements had partial line of sight for five different runs. The receiver was placed at various locations from the transmitter at different distances. Three power levels were again

measured at each distance by moving the receiver left or right from a center point. During all runs the transmitter height was 1.6 meters and the receiver height was 1.1 meters.

Experiment 2 had different settings for each measurement. “Partial” means that there was only partial line of sight. Each of the runs completed during this experiment was influenced by several factors. In the hangar, the transmitter and receiver were placed in positions where different components of nearby aircraft partially or completely blocked the signal. Figures 5.8-5.11 show LOS and NLOS data and the CI model for the hangar environment at 31 GHz. Figure 5.12 shows the CI model for all data combined in 5.8-5.11.

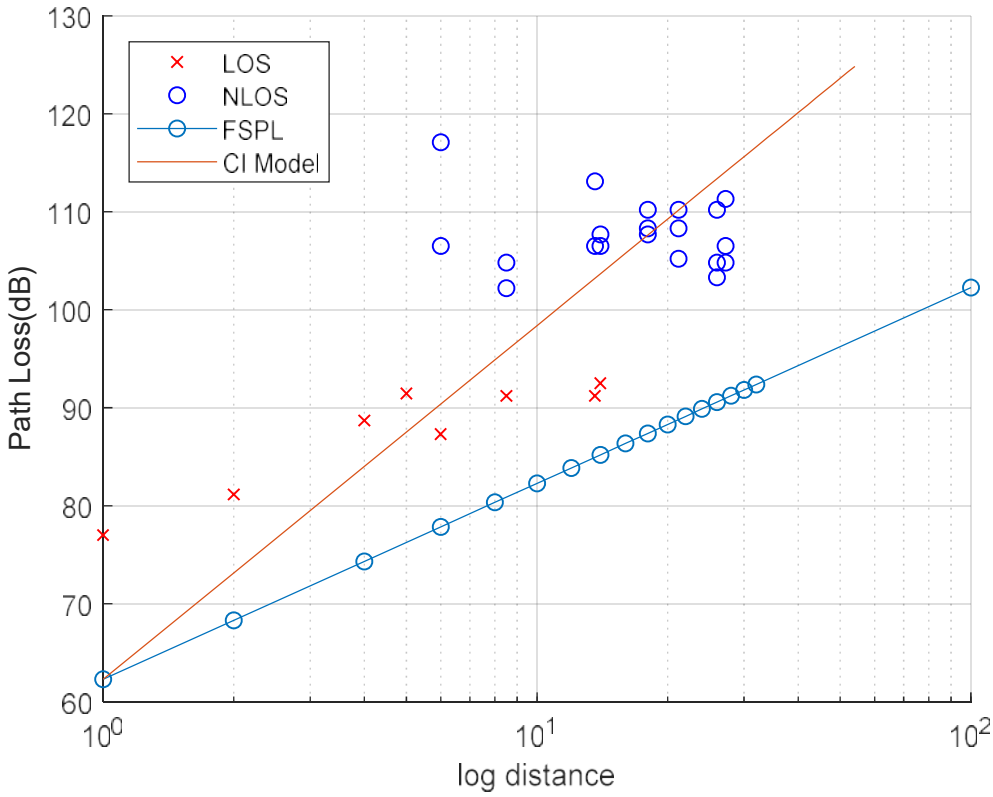

Figure 5.8. Measured path loss data, CI model for combined LOS/NLOS path loss, and Free Space path loss vs. the logarithm of distance in Hangar at 31 GHz, Run 1.

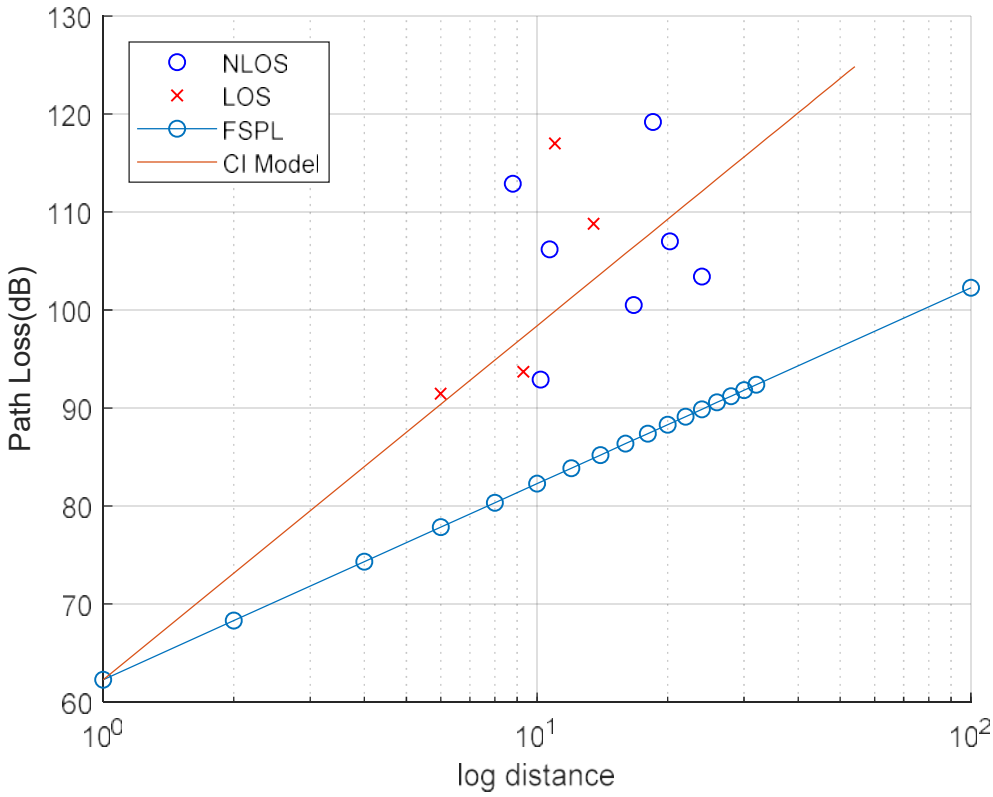

Figure 5.9. . Measured path loss data, CI model for combined LOS/NLOS path loss, and Free Space path loss vs. the logarithm of distance in Hangar at 31 GHz Run 2.

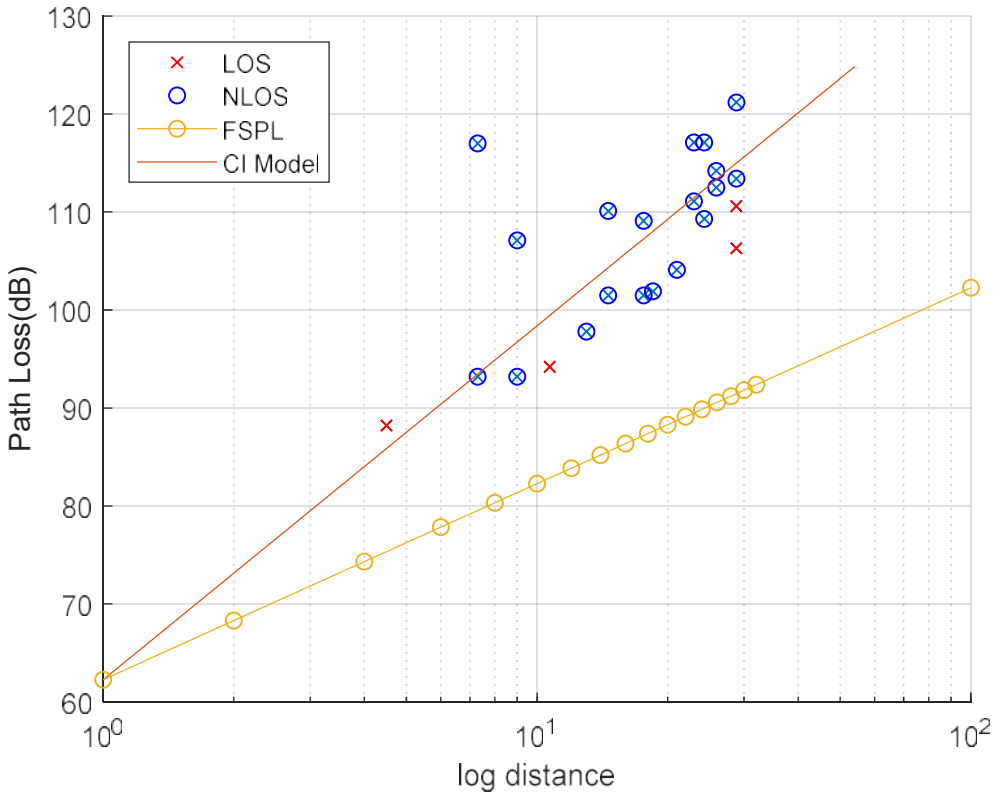

Figure 5.10. Measured path loss data, CI model for combined LOS/NLOS path loss, and Free Space path loss vs. the logarithm of distance in Hangar at 31 GHz Run 3.

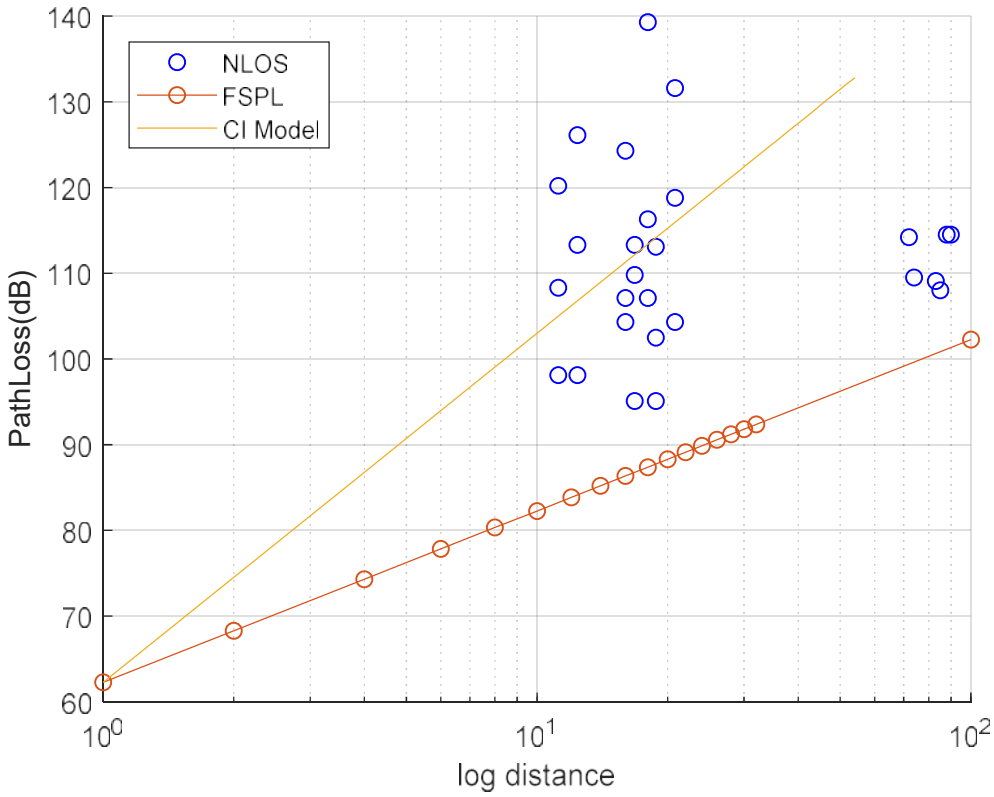

Figure 5.11 . Measured path loss data, CI model for combined LOS/NLOS path loss, and Free Space path loss vs. the logarithm of distance in Hangar at 31 GHz Run 4.

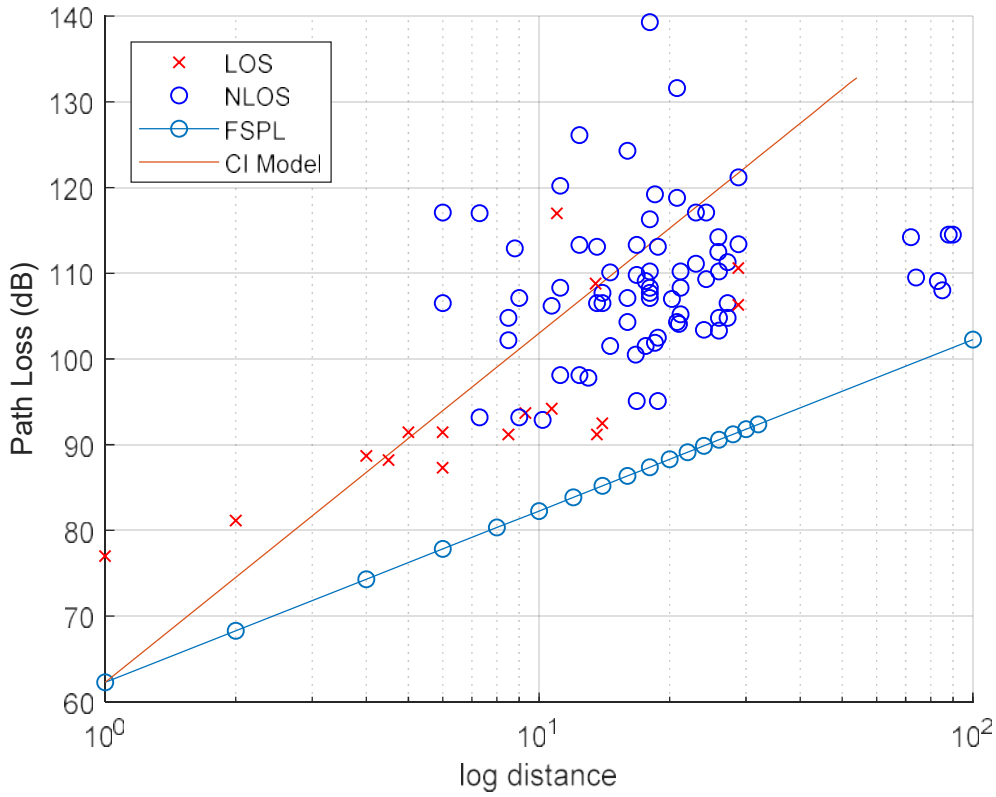

Figure 5.12. All measured path loss data, CI path loss model for combined data of four previous LOS/NLOS measurements, s and Free Space path loss vs. the logarithm of distance at 31 GHz.

The LOS path loss data slopes are actually close to that of free space, but there is still an offset, with measured values on the order of 10 dB larger than free space path loss. Because of the grouping of LOS with NLOS data, and also because the CI model forces the intercept to be the free space loss at the reference distance of 1 m, the CI model slopes are all larger than 2. The fit standard deviation of 8.92 dB for the combined data is comparable to that found in [2]. CI model parameters are listed in Table 5.2.

Table 5.2 CI path loss model parameters, standard deviation and path loss exponents, of all hangar runs.

Run	**σ (dB)**	**n**
1	10.16	3.75
2	9.52	4.68
3	8.92	3.92
4	10.55	4.81

CHAPTER 6

CONCLUSION

Wireless measurements in the millimeter wave band at 31 GHz were taken at the Jim Hamilton–L. B. Owens Airport in Columbia, SC, for both LOS and NLOS settings. Transmitter locations included inside the terminal building on both floors, and inside a maintenance hangar. Path loss models were computed as a function of distance for each setting. The model fit standard deviation values σ for the hangar were larger than those found in the New York measurements [2]. The largest standard deviation from [2] was 8.7 dB, whereas the range of σ for the hangar was from 8.92 to 10.95 dB. Standard deviations for inside the terminal building ranged from 5.45 to 7.03 dB, which is lower than values for the NLOS measurements in [2]. The path loss model slopes found in this work, and in [2], were greater than the free space path loss value of 2. The models in this paper may be used for design of future wireless systems that will be deployed in similar airport settings.

Future work should include first, a careful re-analysis of the data to correct miscalibrations. Second, additional measurements should be taken in other airport settings to expand the database, and cover additional airport environment conditions.

REFERENCES

[1] V. K. Nassa, "Wireless Communications: Past, Present and Future," *Dronachary Research Journal*, vol. iii, issue ii, 2011.

[2] S. Rangan, "Millimeter-Wave Cellular Wireless Networks: Potentials and Challenges," *Proceedings of the IEEE*, vol. 102, issue 3, March 2014.

[3] K Sakaguchi, "Where, When, and How mmWave is Used in 5G and Beyond," *IEICE Trans Electron*, vol E1100-C, no. 10, Oct. 2017.

[4] M. Khatun, H. Mehrpouyan "60-GHz Millimeter-Wave Pathloss Measurements in Boise Airport," *IEEE/AIAA 36th Digital Avionics Systems Conference (DASC),* St. Petersburg, FL, Sep. 17, 2017.

[5] "Long Term Evolution (LTE) Public Safety Information Sheet," FCC, 2009.

[6] S. Sur, V Venkateswaran, "60 GHz Indoor Networking through Flexible Beams: A Link-Level Profiling," 2015

[7] Z. Pi, F. Khan "An Introduction to Millimeter-Wave Mobile Broadband Systems," *IEEE Communications Magazine,* vol. 49, issue 6, page 8, June 2011.

[8] E. Hecht, *Optics* 4th ed., Addison-Wesley, Boston, MA, 2001.

[9] J. Seybold, *Introduction to RF Propagation*, Wiley, Hoboken, NJ, 2005.

[10] D. W. Matolak, University of South Carolina Lecture Notes, ELCT 562 course, Wireless Communications, 3 February 2018.

[11] D. W. Matolak, University of South Carolina Lecture Notes, ELCT 562 course, Wireless Communications, 15 February 2018.

[12] G. R. Maccartney, T. S. Rappaport, "Indoor Office Wideband Millimeter-Wave Propagation Measurements and Channel," *IEEE Access,* volume 3, 2015.

[13] M. Comiter, M. Crouse, "Millimeter-wave Field Experiments with Many Antenna Configurations for Indoor Multipath Environments," *IEEE Globecom Workshops* (GC Wkshps), Cambridge, MA December 4, 2017.

[14] M. Khatun, H. Mehrpouyan, "Millimeter Wave Systems for Airports and Short-Range Aviation Communications: A Survey of the Current Channel Models at mmWave Frequencies," *IEEE/AIAA 36th Digital Avionics Systems Conference (DASC)*, St. Petersburg, FL, Sep. 17, 2017.

[15] M. Park, H. K. Pan, “Effect of device mobility and phased array antennas on 60 GHz wireless networks,” *mmCom '10*, Chicago, IL, 2010.

[16] S. Karthika, “Path Loss Study of Lee Propagation Model,” *International Journal of Engineering and Techniques,* vol. 3, issue 5, Sep-Oct 2017.

Appendix A: Photographs of Equipment used in all Experiments

In this appendix, we provide photographs of the equipment used in the path loss measurements. Equipment model information is provided in Chapter 4.

Figure A.1. Photograph of signal and spectrum analyzer (left) and vector signal generator (right).

Figure A.2. 31 GHz Horn Antenna.

Figure A.3. Microwave Dynamics Amplifier.

Figure A.4. 5 GHz Omni-directional Antenna.

Figure A.5. Microwave Dynamics Mixer.

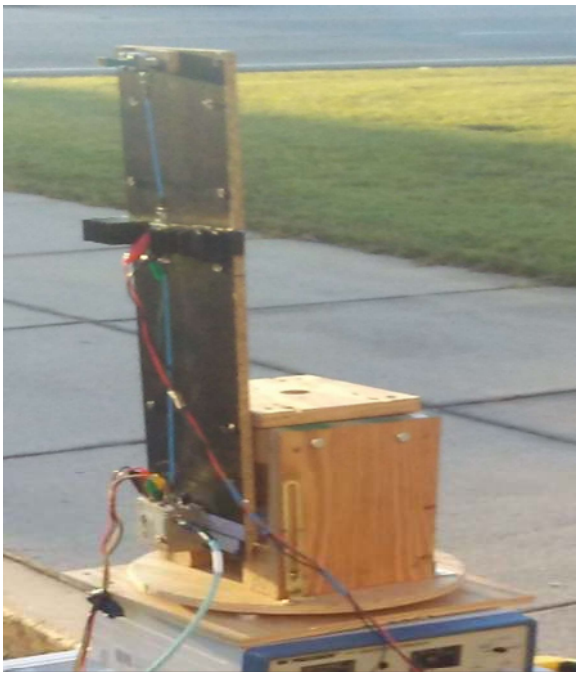

Figure A.6. Antenna mount set up for Transmitter.

Figure A.7. Cart with Receiver Equipment and Power Supplies.

Figure A.8. 1500 W Power Inverter.

Figure A.9. Marine 12 V DC Battery.

Appendix B: Tables for pre-test, Airport, Main Building and Hangar Measurements

In this appendix, we provide all data measured in the experiments described in chapters 3 and 5. The tables that follow are in chronological order, beginning with pre-airport test measurement data and ending with the hangar power measurement data.

Table B.1 Received Power in dBm vs. distance in meters (Swearingen Parking Lot at 31 GHz for co-polarized setting).

Outdoor 31 GHz Co-polarized measurement	
Power (dBm)	distance (m)
-45	2
-52	4
-54	6
-56.2	8
-59.5	10
-61.3	12
-62.3	14
-61.8	16
-64.7	18
-65.2	20
-66.4	22
-67.2	24
-65.2	26
-69.2	28
-72.6	30
-76.3	32
-67.5	34
-71.2	36
-73.4	38
-72.3	40

-74.6	42

Table B.2 Received Power in dBm vs. distance in meters (Swearingen Parking Lot at 31 GHz for cross-polarized setting).

Outdoor 31 GHz Cross-polarized Measurement	
Power (dBm)	distance (m)
-24	2
-35	4
-37.6	6
-39.4	8
-40.6	10
-41.4	12
-43.3	14
-42.8	16
-44.3	18
-46.8	20
-47.5	22
-48.1	24
-46.9	26
-48.2	28
-57	30
-60.6	32
-52	34
-56	36
-53.2	38
-56.2	40
-54.9	42

Table B.3 Received Power (dBm), Average Power (dBm), and Free space path loss (dB) vs distance in meters in Hallway at 5 GHz.

		5 GHz Hallway Data (LOS)			
distance (m)	data 1 (dBm)	data2 (dBm)	data 3 (dBm)	avg data	FSPL (dB)
2.2	-39.4	-42.2	-39.7	-40.2652846	53.26
4.2	-41.9	-40.6	-46.7	-42.3897123	58.88
6.2	-44.3	-42.9	-43	-43.3548844	62.26
8.2	-46.7	-45.7	-44.8	-45.6645374	64.7
10.2	-48.9	-49	-46.9	-48.1541144	66.59
12.2	-45.8	-47.8	-46.9	-46.7560828	68.15
14.2	-48.7	-49.7	-46.8	-48.2296606	69.47
16.2	-51.2	-52.1	-50.9	-51.3707332	70.61
18.2	-45.8	-46.5	-46.8	-46.3461903	71.62
20.2	-56.8	-53.8	-51.8	-53.6771401	72.52
22.2	-53.9	-53.8	-51.8	-53.0541144	73.35
24.2	-49.8	-49.4	-51.2	-50.0673138	74.1
26.2	-54.7	-53.9	-54.1	-54.2202225	74.78

Table B.4 Received Power (dBm) and Average Power (dBm) vs. distance in meters for Hallway at 31 GHz.

		Indoor LOS at 31 GHz		
Power (dBm)	Power (dBm)	Power (dBm)	average	distance (m)
-28.3	29.6	-30.1	-29.2654758	1
-31.8	-32.2	-33.3	-32.3882715	4
-34.3	-34	-38.3	-35.1448998	6
-37.5	-37.8	-41.8	-38.6448998	8
-41.9	-40.8	-37.6	-39.6991072	10
-39.7	-51.8	-41.	-41.9113282	12

-47.6	-45.2	-43.4	-45.0730318	14
-47.3	-44.5	-53.2	-47.0709068	16
-44.6	-47.3	-47.5	-46.2539002	18
-41.7	-41.2	-44.5	-42.2439588	20
-49.8	-53.6	-51.4	-51.3310638	22
-47.7	-51.7	-52.1	-50.0131622	24
-44.6	-42.8	-39.3	-41.6612184	26

Table B.5 Loss in dBm vs. distance in meters in Airport terminal building at 31 GHz for Run #1.

	Run # 1 Indoors LOS		
Loss (dB)	Loss (dB)	Loss (dB)	distance (m)
82.2	83.3	83.1	2
86.8	87.6	87.3	4
88	92.4	91.8	6
95.9	96.8	90.7	8
96.1	95	94.9	10
98.5	100.7	98.2	12
100.5	98.5	98.2	14

Table B.6 Loss in dBm vs. distance in meters in Airport terminal building at 31 GHz for Run #2.

	Run # 2 indoor LOS		
Loss (dB)	Loss (dB)	Loss (dB)	distance (m)
83.3	82.8	84.1	2
88.8	88.6	89.4	4
89.7	92.1	93.2	6
93.8	95.9	96.3	8
92.4	95.9	96.8	8
101.7	95.2	97.5	10

Table B.7 Loss in dBm vs. distance in meters in Airport terminal building at 31 GHz for Run #3.

	Run # 3 indoor LOS		
Loss (dBm)	Loss (dB)	Loss (dB)	distance (m)
83	83.3	84.2	2
90.5	89.9	89.3	4
90.3	93.8	95.9	6
93.9	91.7	95.4	8

Table B.8 Power in dBm vs. distance in meters in Airport terminal building at 31 GHz for Run #4.

	Run # 4 Indoor NLOS same floor			
Power (dBm)	Power (dBm)	Power (dBm)	distance (m)	location
-54.8	-63.7	-56.4	11.8	Vending
-62.1	-59.3	-59.9	12.7	Bathroom
-52.3	-51.8	-51.9	8.7	TV room
-51.7	-53.4	-52.8	10.3	Tv room
-51.6	-46.9	-50.8	6.9	PC room
-46.9	-53.5	-52.8	7.3	PC room
-50.9	-43.5	-42.3	3.2	book room

Table B.9 Measured Power in dBm vs. distance in meters in Airport terminal building at 31 GHz for Run #5.

	Run # 5 Indoor NLOS different floor			
Power (dBm)	Power (dBm)	Power (dBm)	distance (m)	location
-56.8	-56.9	-57.8	5.7	Main Hall
-65.8	-67.3	-66.9	3.2	book room
-68.4	-61.9	-66.8	6.9	PC room
-67.1	-69.4	-69.2	7.3	PC room
-66.6	-65.7	-64.4	8.7	TV room
-67.5	-65.3	-67.3	10.3	TV room
-55.8	-60.9	-65.5	8.3	Behind stairs
-47.4	-45.6	-49.2	9.3	Behind stairs

Table B.10 Measured Power in dBm vs. distance in meters at Hangar for 31 GHz LOS Run #1.

	Run 1 (LOS)
distance(m)	P(dBm)
1	-20
2	-24.15
4	-31.7
5	-34.45

Table B.11 Measured Power in dBm vs. distance in meters at Hangar for 31 GHz NLOS Run #1.

	Run 1 (NLOS)
distance (m)	Power(dBm)
8.8	-55.9
11	-60
13.5	-51.8
18.5	-62.2
20.24	-50
24	-46.4

Table B.12 Measured Power in dBm vs. distance in meters at Hangar for 31 GHz Run #2.

		Run 2	
setting	distance(m)	Pmin	Pmax
los	6	-30.3	-34.2
partial	8.5	-35.5	-51.3
partial	13.6	-46.3	-49.5
partial	14	-45.2	-49.5
partial	18	-53.2	-53.2
partial	21.2	-54.3	-60.1
nlos	26	-56.1	-50.7
nlos	27.2	-48.2	-47.8

Table B.13 Measured Power in dBm vs. distance in meters Hangar for 31 GHz Run #3.

		Run 3	
setting	distance(m)	P(dBm)	P(dBm)
los	4.5	-31.2	-27.7
partial	10.7	-37.2	-37.2
partial	13	-40.8	-41.3
partial	18.5	-44.9	-43.8
partial	21	-47.1	-45.2

Table B.14 Measured Power in dBm vs. distance in meters Hangar for 31 GHz Run #4.

	Run 4	
setting	distance(m)	Power(dBm)
los	6	-34.46
partial	9.3	-36.7
partial	10.2	-35.9
partial	10.7	-49.2
partial	16.7	-43.5

Table B.15 Measured Power in dBm vs. distance in meters Hangar for 31 GHz Run #5.

	Run 5	
dist (m)	P (dBm)	Power(dBm)
7.3	-36.2	-37.1
9	-44.5	-44.8
14.6	-60.1	-59.3
17.6	-53.6	-49.3
23	-55.5	-60
24.3	-50.1	-53.1

28.8	-52.1	-54.1
28.8	-52.3	-56.4
25.9	-64.2	-57.2

Table B.16 Measured Power in dBm vs distance in meters Hangar for 31 GHz Run #6.

	Run 6	
dist(m)	Power(dBm)	Power(dBm)
11.2	-41.1	-41.1
12.4	-38.1	-38.1
16.8	-61.8	-50.1
18.8	-51.3	-56.3
20.8	-45.5	-47.3
16	-59.3	-63.2
18	-52.8	-56.1